YANG, CHUE HUE, M.S. Detection and Sequencing of MicroRNA using MALDI Time-of-Flight Mass Spectrometry. (2010)
Directed by Dr. Norman H. L. Chiu. 57 pp.

The discovery of microRNAs (miRNAs) and their abilities to regulate *in vivo* protein synthesis have led to growing interests in miRNA research. Due to their functions on regulating cellular processes that are related to diseases such as cancer, miRNAs can potentially become a new class of diagnostic biomarkers and therapeutic agents. Since early 2000, researchers have reported more than 1,000 human miRNAs. To facilitate high-throughput clinical studies, there are needs for more accurate and robust analytical methods to detect and quantitate miRNAs. Matrix-assisted laser desorption/ionization time-of-flight mass spectrometry (MALDI-TOF MS) has been used mainly for proteomics research. In the past two decades, MALDI-TOF MS has also been used in genomics research. Specifically, MALDI-TOF MS has been used in the analysis of oligonucleotides, both DNA and RNA. In this study, the use of MALDI-TOF MS to detect specific miRNA was optimized, and the applicability of tandem MALDI-TOF/TOF to perform partial *de novo* sequencing was evaluated.

The MALDI process requires a small organic compound, often known as "matrix", which readily undergoes desorption on contact with UV laser and assists the ionization of analyte. Therefore, an investigative study was designed to compare five commonly used MALDI matrix compounds for oligonucleotide analysis. The selected matrix compounds includes 3-hydroxypicolinic acid (3-HPA), 2',3',4'-trihydroxy-acetophenone (THAP), 6-aza-thiothymidine (6-ATT), 3,4-diaminobenzophenone (DABP) and 3-hydroxycoumarin (3-HC). The goal is to identify which is the best matrix

for supporting the MALDI process and the subsequent tandem MALDI-TOF/TOF measurements. The 4700 Applied Biosystems Proteomics Analyzer was initially used to perform linear MALDI-TOF MS analysis of a selected microRNA standard (miR-124a). The initial results of our MS/MS measurements indicated higher signal intensity or ion count of the parent ion of miRNA is required to achieve sequencing. For this reason, we embarked on a series of studies to increase the signal intensity, especially on the effects of various parameters that were related to the desorption of miRNA during the MALDI process. The results indicated 3-HPA matrix has provided the highest signal intensity. Thus, 3-HPA was used to further optimize the MALDI-TOF MS measurements of miRNA. Once the parameters of MALDI-TOF MS were optimized, the use of tandem MALDI-TOF/TOF MS to perform partial *de novo* sequencing of miRNA was evaluated. Following the acquisition of initial MS/MS spectra of miR-124a, the use of different collision-induced dissociation (CID) pressures and delayed times to induce the fragmentation of miR-124a parent ion were investigated. It was determined that the 4700 Proteomics Analyzer could have a limitation on measuring the singly-charged miR-124a parent ion (7,161 *m/z*). This could be due to the current design and/or settings on the reflectron within the MALDI-TOF/TOF instrumentation were not suitable for measuring ions with high molecular masses. To overcome this limitation, the doubly-charged miR-124a parent ion (3,582 *m/z*) was selected as an alternative for performing the tandem MALDI-TOF/TOF MS measurements. Both post-source decay (PSD) and CID in the positive ion mode were used.

DETECTION AND SEQUENCING OF MICRORNA USING MALDI TIME-OF-FLIGHT MASS SPECTROMETRY

by

Chue Hue Yang

A Thesis Submitted to
the Faculty of The Graduate School at
The University of North Carolina at Greensboro
In Partial Fulfillment
of the Requirements for the Degree
Master of Science

Greensboro
2010

Approved by

_____
Committee Chair

APPROVAL PAGE

This thesis has been approved by the following committee of the Faculty of The Graduate School at The University of North Carolina at Greensboro.

Committee Chair _____

Committee Members _____

_____

_____

Date of Acceptance by Committee

_____

Date of Final Oral Examination

ACKNOWLEDGMENTS

I wish to thank Dr. Norman H. L. Chiu for his superior mentorship and guidance. I also wish to thank my committee members, Dr. Nadja Cech and Dr. Greg Raner, for their feedback and advices. I wish to thank Banner Pharmacaps, Inc. for financial support through their education assistantship program. Furthermore, I wish to thank the Department of Chemistry and Biochemistry of UNCG for the great faculty and facilities.

TABLE OF CONTENTS

Page

LIST OF TABLES vi

LIST OF FIGURES vii

CHAPTER

I. INTRODUCTION 1

II. EXPERIMENTAL METHODS AND MATERIALS 7

Preparation of matrix solutions 8
Preparation of miR-124a sample 9
Thin- layer MALDI sample preparation method 9
Dried droplet MALDI sample preparation method 9
MALDI-TOF MS measurements 9
MALDI-TOF/TOF MS/MS measurements 10
Effects of laser intensity on measuring 3-HPA matrix 12
Effects of laser intensity on measuring miR-124a 12
Effects of increasing miR-124a concentration 13
Thin-layer versus dried droplet sample preparation method 13
Hydrophobicity of matrix compounds 13
Solubility of matrix compounds 13
Drying time for selected matrix compounds 14
UV absorbance of selected matrix compounds 14
Preparation of MALDI samples 15
“Spiking” experiment with 3-HPA matrix 15

III. RESULTS AND DISCUSSION 17

Effects of laser intensity on measuring 3-HPA matrix 22
Effects of laser intensity on measuring miR-124a 24
Effects of increasing miR-124a concentration 26
Thin-layer versus dried droplet method 28
Hydrophobicity of matrix compounds 29
Solubility of selected matrix compounds 31
Drying time of selected matrix compounds 33
UV absorbance of selected matrix compounds 34

Co-crystallization of MALDI matrix with miR-124a 36
"Spiking" experiment with 3-HPA matrix 38
Investigation of MALDI-TOF MS/MS parameters 40
Sequence analysis of miR-124a 47

IV. CONCLUSIONS 53

REFERENCES 55

LIST OF TABLES

Page

Table 1. Five commonly used matrix compounds in oligonucleotide analysis 8

Table 2. 3-D structure and Log P value of matrix compounds 31

Table 3. Solubility of matrix compounds in 50% ACN:H_2O and 50% DMF:H_2O 32

Table 4. Drying time of 0.2 M matrix solutions prepared in 1 mL 50% DMF:H_2O solvent 34

Table 5. Extinction coefficient of matrices at 355 nm wavelength 35

Table 6. Photograph of dried matrix spots prepared in 50% DMF:H_2O 37

Table 7. Summary of 3-HPA "spiking" study to optimize *S/N* ratio 40

Table 8. Identification of (a-w) fragment ions by comparing measured masses to theoretical masses of expected fragment ions 49

Table 9. Identification of (c-y) fragment ions by comparing measured masses to theoretical masses of expected fragment ions 51

LIST OF FIGURES

Page

Figure 1. Schematic diagram of 4700 Applied Biosystems Proteomics Analyzer 5

Figure 2. MALDI mass spectrum of 20 μM miR-124a 18

Figure 3. Schematic of possible fragmentation sites on RNA oligonucleotide structure 19

Figure 4. Initial MS/MS spectrum of 25 μM miR-124a 21

Figure 5. (a) MALDI mass spectrum of 3-HPA matrix, and (b) effects of laser intensity on signal-to-noise (S/N) ratio and ion count of 3-HPA matrix ion 23

Figure 6. (a) MALDI mass spectrum of 20 μM miR-124a, and (b) effects of laser intensity on signal-to-noise (S/N) ratio and ion count of $[\text{miR-124a} + H^+]^+$ ion 25

Figure 7. (a) MALDI mass spectra of miR-124a at different concentrations, and (b) effects of miRNA concentration on its corresponding signal-to-noise (S/N) ratio and ion count in MALDI-TOF MS measurements 27

Figure 8. MALDI mass spectra of 20 μM miR-124a samples that were prepared by using (a) thin-layer method and (b) dried droplet method. 29

Figure 9. UV absorption spectra (200-600nm) of five different matrix compounds prepared in 10% ACN:H_2O and 0.04 M ammonium citrate dibasic solution 35

Figure 10. MALDI mass spectra of 5 μM miR-124a samples that were prepared by using the thin-layer method and different matrix compounds 39

LIST OF FIGURES

Page

Figure 11. MS/MS spectra of [miR-124a + H^+]$^+$ at (a) positive and (b) negative ion mode. 41

Figure 12. MS/MS spectra of [miR-124a + H^+]$^+$ ion that were acquired at different CID pressure, $1.0e^{-07}$ – $8.0e^{-06}$ Torr....44

Figure 13. MS/MS spectra of [miR-124a + H^+]$^+$ that were acquired with low (a) and high (b) duration times for the CID process 45

Figure 14. MS/MS spectrum of [miR-124a + $2H^+$]$^{2+}$ precursor ion and its fragment ions 46

Figure 15. MALDI mass spectrum of [miR-124a + $2H^+$]$^{2+}$ ion that was acquired by using the mode of post-source decay. 47

Figure 16. MS/MS spectra of [miR-124a + $2H^+$]$^{2+}$ precursor ion, with selected (a-w) fragment ions being highlighted....50

Figure 17. MS/MS spectra of [miR-124a + $2H^+$]$^{2+}$ precursor ion, with selected (c-y) fragment ions being highlighted....52

CHAPTER I

INTRODUCTION

Mature microRNAs (miRNAs) are small ribonucleic acid molecules, usually composed of ~19-25 ribonucleotides that are responsible for the regulation of protein synthesis[1]. miRNAs are found in a wide variety of plant and animal cells, serving as post-transcriptional regulators that bind to complementary sequences of the three prime untranslated regions (3' UTRs) of target messenger RNA (mRNA). miRNAs originate from miRNA genes found in introns or exons of protein and non-protein coding genes, containing their own miRNA gene promoter and regulatory units, which allow transcription to occur. Within the nucleus, RNA polymerase II binds to the gene promoter and transcribes miRNA genes into primary miRNAs (pri-miRNAs). The resulting pri-miRNA transcript has a hairpin loop structure that contains a specially-modified 5' cap and a poly(A) tail at the 3' end. Drosha-Pasha complex in the nucleus cleaves the pri-miRNA near the hairpin stem into a 70-90 nucleotide (nt) stem-loop called premature miRNA (pre-miRNA)[2]. The pre-miRNA product is then exported by Exportin 5 into the cytoplasm, where it is further cleaved into a short miRNA duplex by RNase III Dicer. One of strands in the miRNA duplex is rapidly degraded, leaving only a single-stranded mature miRNA. The mature miRNA associates with the RNA-induced silencing complex (RISC) and targets the 3' UTR of mRNAs by partial annealing. The miRNA-RISC regulates protein synthesis by repressing the translation of mRNA or

causes mRNA degradation[3].

microRNAs were first discovered while studying *Caenorhabditis elegans* through genetic analysis of developmental mutants. It was observed that small RNAs were responsible for inhibiting the translation of *lin*-14 mRNA into LIN-14 protein within *C. elegans* during its developmental stage transition[4]. Since the early 2000s, the study of microRNAs has gained a lot of interests for its applications in therapeutic treatments against human diseases such as cancer, diabetes and regulation of the nervous system, providing many models for the continuous study of these biomolecules. In 2007, an investigation of cyclin G1 was found to be a target of miR-122a, microRNA frequently down-regulated in human hepatocellular carcinoma[5]. miR-122a was shown to modulate cyclin G1 expression in HCC-derived cell lines. miR-21 is shown to be over expressed in tumor tissues compared with the matched normal tissues and the suppression of miR-21 by antisense oligonucleotides inhibits tumor cell growth[6]. miRNAs function as suppressors/regulators during transcription to inhibit the production of proteins required for the life cycle of diseases. The ideology of miRNA regulation of diseases promoted the drive to identify them. A database was created for miRNAs that have been identified from several plant and animal species, most importantly the miRNAs from *Homo sapien*s. The human genome may encode over 1,000 miRNAs, but only 940 miRNAs have been isolated to date[7]. There are 940 miRNAs isolated from the human body, but only a few are associated with cancerous diseases of the brain. Our study focuses on brain cancer miRNAs, which regulate the development of brain cancer cells.

Nucleic acid research has attracted many researchers to develop methods for

analyzing nucleic acids including various types of RNA. These methods, in turn, have been applied to the study of miRNAs. A problematic issue for the analysis of miRNA is the availability of sample. Most methods usually require hundreds of micrograms of total RNA for sample preparations, while tissue-derived RNA that are obtained from a clinical biopsy sample may only yield nano- or pico- gram levels of sample[8]. The most commonly used approaches for miRNA identification and quantification include reverse transcriptase-polymerase chain reaction (RT-PCR) and microarray-based methods. A novel miRNA quantitation method has been developed using stem-loop primer for reverse transcription and followed by TaqMan PCR analysis to achieve a precise quantification of specific miRNA in 25 pg of total RNA, which enables fast, accurate and sensitive miRNA expression profiling and can identify and monitor potential biomarkers specific to tissues or diseases[9]. A novel miRNA profiling microarray was reported, in which miRNAs were directly labeled at the 3' terminus with biotin and hybridized with complementary oligo-DNA probes immobilized on glass slides, and subsequently detected by measuring fluorescence of quantum dots that have been conjugated to streptavidin molecule, which is bound to miRNAs through streptavidin-biotin interaction[10]. These reported procedures allow for low miRNA detection limits, but requires extensive preparations and resources. To further improve the accuracy for miRNA analysis, the research work in this thesis has focused on using matrix-assisted laser desorption/ionization mass spectrometry (MALDI MS) to identify and sequence specific miRNA biomarkers.

Although many RNA analytical methods exist in the literature there is minimal focus towards miRNA analysis by using MALDI MS. In a recent publication by Barnes and Chiu[11], a method was developed for the analysis of carcinogenic DNA adducts using MALDI MS. This provided an in-sight for miRNA sample preparations and analysis using MALDI MS, due to the structural similarities of DNA and RNA. MALDI tandem time-of-flight (TOF) MS has been used to detect and sequence 4-mer RNA sequences[12]. Several 4-mers with different sequences were used in that study. The 4-mers were fragmented into single nucleotides and provided spectral data for sequence analysis. This study showed that short RNA sequences could be detected and sequenced through the MALDI MS, providing the possibility to explore and use MALDI MS to detect and sequence larger RNA molecules such as miRNAs. The focus of our research is to provide a method for the analysis and partial sequencing of pure synthetic miRNA using MALDI-TOF MS/MS, with a long-term goal to characterize specific miRNAs in biological samples.

Matrix-assisted laser desorption/ionization time-of-flight mass spectrometry (MALDI-TOF MS) is an analytical technique for determining the mass-to-charge (*m/z*) ratio of an analyte through a process of creating molecular ions of the analyte and uses the *m/z* ratio to generate spectral data for identifying the analyte. MALDI is the initial process that is crucial for generating sufficient ions for analysis. This process requires a matrix compound that is compatible with the analyte. The matrix compound must absorb UV laser readily for generating sufficient molecular ions. The generated analyte ions are then drawn into the time-of-flight mass analyzer, in which the ions are separated by *m/z*

ratios. The linear ion detector is used for MALDI-TOF MS, where ions travel in a linear path to the detector and generate the signals in the corresponding mass spectrum. The linear MS process can be carried out further to perform the fragmentation of parent ion, through MALDI-TOF MS/MS.

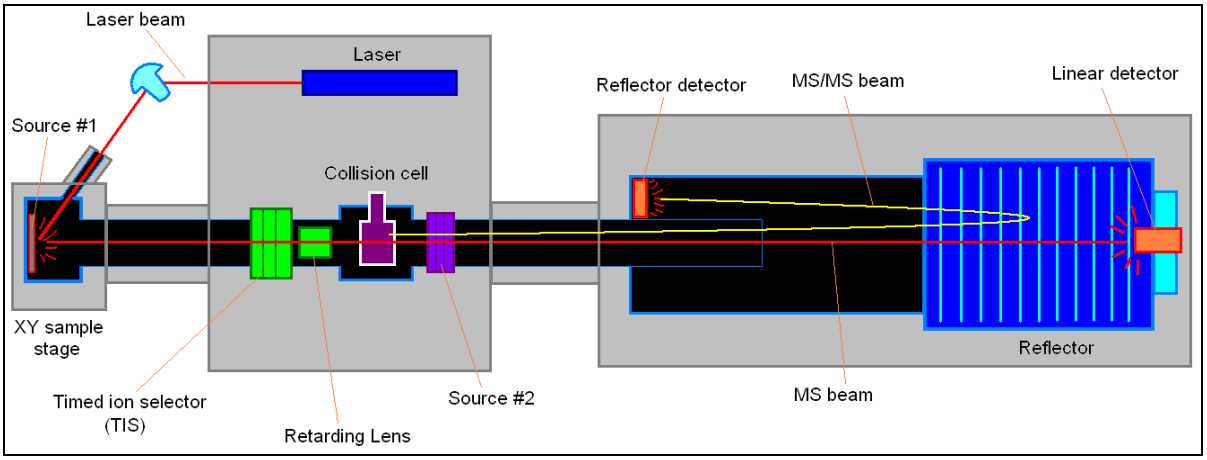

Figure 1. Schematic diagram of 4700 Applied Biosystems Proteomics Analyzer.

MALDI-TOF/TOF MS/MS is based on collision-induced dissociation (CID). In this study, MS/MS is used to determine the RNA sequence that makes up the primary structure of miRNA. Through the MS/MS process, the parent ions that were generated in linear MS mode are selected by specifying a mass window to isolate the parent ion for CID fragmentation. The parent ion is isolated in a collision cell where fragmentation is taken place. Once inside the collision cell, with the higher gas pressure, the parent ions are bombarded with gas molecules. The collision of gas molecules with the parent ions induces ion fragmentation. The CID fragments are subjected to the second time-of-flight mass analyzer, where fragment ions are resolved. Fragments containing more kinetic

energy travel faster and penetrate further into the grid of increasing opposite potential in the reflectron, while fragments with less kinetic energy travel slower and shorter distance in the reflectron. The difference in travel distance allows for compensation in difference in kinetic energies. The fragment ions are then reflected towards the reflectron ion detector. The spectrum generated from CID fragmentation can be used to determine the sequence of miRNA analyte.

The focus of our research group is towards the analysis of miRNAs. Therefore, synthetic RNA oligonucleotide was used as a control to build a foundation for our long term goal. Fortunately, our departmental facilities include a MALDI-TOF/TOF MS (4700 Applied Biosystems Proteomics Analyzer), which is equipped with laser energy to analyze and fragment RNA oligonucleotides for potential sequencing. MALDI-TOF MS has been used to analyze and sequence shorter RNA oligonucleotides, but for our research we focus on relative long RNA that has at least 19 ribonucleotides. The analysis of such a larger biomolecule requires the evaluation and/or development of new and robust analytical method for using MALDI-TOF MS. In addition, our task has also included the partial sequencing of miRNA molecule.

CHAPTER II

EXPERIMENTAL METHODS AND MATERIALS

A list of five matrix compounds, commonly used for oligonucleotide analysis through literature search, was compiled for matrix comparison study (Table 1). For MALDI mass spectrometry of DNA, 3-HPA is one of the most commonly used MALDI matrices reported in a study of carcinogenic DNA adducts[11]. A mixture of 2',4',6'-trihydroxyacetophenone, 2',3',4'-trihydroxyacetophenone and ammonium citrate with molar ratios of 2:1:1 serves as a good matrix for the detection of DNA was reported[13]. In 2006, a new matrix of 3,4-diaminobenzophenone was demonstrated to be advantageous in the analysis of oligonucleotides by MALDI-TOF MS[14, 15]. 3-hydroxycoumarin was designed, synthesized, and tested as a matrix for MALDI-TOF MS analyses of a variety of synthetic oligodeoxynucleotides ranging from 3-70 bases[16]. 6-aza-2-thiothymine matrix and dibasic ammonium citrate were mixed with a montmorillonite catalyst for direct MALDI-MS analyses of synthesized oligonucleotides[17, 18].

Table 1. Five commonly used matrix compounds in oligonucleotide analysis.

Matrix Compound	Reference
3-hydroxy picolinic acid (3-HPA)	Subbi, J Barnes, C Kim, Y Fu, Y
2',3',4'-trihydroxyacetophenone (THAP)	Andersen, T Zhu, Y Fu, Y
3,4-diaminobenzophenone (DABP)	Fu, Y Xu, S
3-hydroxycoumarin (3-HC)	Zhang, Z
6-aza-2 thiothymine (6-ATT)	Zagorevskii, D Song, F

Preparation of matrix solutions

All matrix compounds: 3-hydroxypicolinic acid (3-HPA), 2',3',4'-trihydroxyacetophenone (THAP), 3,4-diaminobenzophenone (DABP), 3-hydroxy coumarin (3-HC) and 6-aza-2-thiothymine (6-ATT) were purchased from Sigma-Aldrich. Ammonium citrate dibasic ≥99.0% was purchased from Fluka. The solvents used was acetonitrile (ACN), HPLC grade, was purchased from Fisher Scientific and anhydrous *N,N*-dimethylformamide (DMF) 99.8% was purchased from Sigma-Aldrich. 50% DMF was prepared using 500 µL of *N,N*-dimethylformamide and 500 µL of autoclaved deionized water. 10% and 50% ACN were prepared using ACN and autoclaved deionized water. 0.25 M 3-HPA matrix solution was prepared by dissolving 35.0 mg of 3-HPA in 1 mL of 10% ACN with 8.80 mg (0.04 M) ammonium citrate dibasic. To completely dissolve all 3-HPA, the mixture was vortexed for at least 1 min. This was followed by filtering the 3-HPA solution with a 0.2 µm syringe filter.

Preparation of miR-124a sample

A pure, synthetic 22-mer RNA oligo (MW = 7,160.3 g/mol) containing 5'-phosphate and 3'-hydroxyl was purchased from Integrated DNA Technologies, Inc.. The miRNA sample containing a total of 0.22 mg miR-124a was reconstituted in autoclaved, deionized water to 100 μM concentration. Aliquots of miR-124a solution were obtained and diluted to the following concentrations, 5 μM, 10 μM, 20 μM and 50 μM.

Thin- layer MALDI sample preparation method

In this method, the sample was prepared by spotting 0.3 μL droplet of matrix solution onto a cleaned and dried stainless steel MALDI sample plate. The matrix was allowed to air dry into thin-layer. A 0.3 μL droplet of miR-124a sample is then spotted onto top of the dried matrix and allowed to air dry.

Dried droplet MALDI sample preparation method

In this method, a premixed sample was prepared by mixing 2 μL of matrix solution and 2 μL of miR-124a sample. A 0.3 μL droplet of the premixed sample is then spotted onto a cleaned and dried stainless steel MALDI sample plate and allowed to air dry.

MALDI-TOF MS measurements

A MALDI-TOF/TOF instrument (4700 Proteomics Analyzer, Applied Biosystems, Framingham, MA) was used for all MS and MS/MS measurements. The

4700 Proteomics Analyzer is equipped with a 355 nm Nd:YAG laser (200 Hz) and 4000 Series Explorer Version 3.0 software. Each sample was measured by using the linear high mass positive mode in the 4000 Series Explorer Version 3.0 software. A focus mass of 7,161 *m/z* was used for the singly-charged miR-124a ion expected from each sample. Laser intensity at 7500 arbitrary units was used. The accelerating voltage was +20.0 kV and grid voltage was +18.8 kV. The instrument was equipped with a 200 Hz digitizer. The sampling bin size was 0.5 ns with an input bandwidth of 500 MHz, and a vertical full scale of 0.20 mV. The linear detector voltage was +2.0 kV. The pressure inside the entire instrument was maintained at the level of 10^{-8} Torr. Each spectrum was automatically acquired by accumulating the results of 2500 shots (25 shots per sub-spectrum) with random edge-biased positioning of each laser shot. MALDI-TOF Linear MS was used to identify and confirm the presence of selected miRNA model in each sample before proceeding to MS/MS measurements.

MALDI-TOF/TOF MS/MS measurements

Each sample was measured using the MS-MS 1 kV positive mode in the 4000 Series Explorer Version 3.0 software. The precursor mass was the molecular mass of the miR-124a, and the mass window was -10.00 Da and +10.00 Da of the precursor mass. Molecular ions were extracted from the ion source after 460 ns delay time. The suppressor for metastable ion was turned off. The accelerating voltage at the ion source was at +8.0 kV, and grid voltage at +6.85 kV. The collision cell was at +7.0 kV. Fragment ions were extracted from the collision cell after 68.8 ms delay time. The

accelerating voltage from the collision cell was at +15.0 kV. The sampling bin size was 1.0 ns with an input bandwidth of 500 MHz, and a vertical full scale of 200 mV. The reflector detector voltage was +2.1 kV. The pressure inside the collision cell was adjusted with atmospheric air to the level of 10^{-7} Torr before the measurements were performed. Each spectrum was automatically acquired by accumulating the results of 2500 shot (25 shots per sub-spectrum) with random edge-biased positioning of each laser shot. By using the Data Explorer Version 4.6 software, resulting mass spectrum was internally calibrated with the most abundant isotopic peaks of precursor ion. Data Explorer was used to convert raw spectrum into centroid spectra to generate *m/z* peak list for sequence analysis. The online Mongo Oligo Mass Calculator version 2.06 was used to calculate the average molecular mass of miR-124a. In the case of singly charged positive ions, all phosphate groups are protonated plus the addition of an extra hydrogen proton for the positive charge. Microsoft Office 2007 Excel software was used to generate the theoretical masses of expected CID fragments of miR-124a. For post-source decay (PSD) measurements, the same parameter settings as the MS/MS measurements described above were used, except the collision cell was turned off and pressure was maintained at 10^{-8} Torr.

The initial attempt to generate MS/MS spectra did not provide sufficient fragment ion signals. In order to increase ion count and *S/N* ratio of fragment ions, optimization of linear MS measurements was systemically carried out. The optimization of linear MS parameters may increase ion count and allow for more fragment ions to be produced during the CID process. To increase the ion count and S/N ratio of $[\text{miR-124a} + H^+]^+$

ion, we investigated the following parameters: effects of laser intensity on measuring 3-HPA matrix, effects of laser intensity on measuring 20 μM of miR-124a, outcome from using higher concentrations of miR-124a, comparison of two different sample preparation methods, and investigation of using five different MALDI matrix compounds.

Effects of laser intensity on measuring 3-HPA matrix

Matrix solution containing 0.25 M 3-HPA, 0.04 M ammonium citrate dibasic was prepared in 10% ACN. 0.3 μL droplets of 3-HPA matrix solution were spotted onto MALDI sample plate, air-dried and analyzed using MALDI-TOF linear MS mode to acquire spectra at different laser intensities (5,000 – 7,900 arb. units). Low mass positive method was used to acquire each spectrum.

Effects of laser intensity on measuring miR-124a

Matrix solution containing 0.25 M 3-HPA, 0.04 M ammonium citrate dibasic was prepared in 10% ACN. 0.3 μL droplets of 3-HPA matrix solution were spotted onto MALDI sample plate, air-dried. 0.3 μL droplet of 20 μM miR-124a sample were spotted on top of a thin-layer 3-HPA matrix, air-dried and analyzed using MALDI-TOF linear MS mode to acquire spectra at different laser intensities (5,000 – 7,900 arb. units). High mass positive method was used to acquire each spectrum.

Effects of increasing miR-124a concentration

miR-124a samples were prepared in concentrations of 5 μM, 10 μM, 20 μM, 50 μM and 100 μM. 0.3 μL droplet of each sample were spotted on 0.25 M 3-HPA matrix thin-layer spots and analyzed using MALDI-TOF as described above, except the laser intensity was fixed at 7,500 arb. units.

Thin-layer versus dried droplet sample preparation method

For the thin-layer method, 0.3 μL of 20 μM miR-124a sample was spotted on 0.25 M 3-HPA matrix thin-layer spots. For the dried droplets method, 2 μL of 20 μM miR-124a sample was premixed with 2 μL of 0.25 M 3-HPA matrix solution, vortexed to mix thoroughly. 0.3 μL droplet of the premixed solution was spotted on the MALDI sample plate and dried. Both sample preparations of miR-124a was analyzed using MALDI-TOF linear MS mode with laser intensity at 7,500 arb. units.

Hydrophobicity of matrix compounds

ACDlabs 12.0 ChemSketch software was used to draw 3-D images of the five matrix compounds. To estimate the hydrophobicity of each matrix compound, the same software was also used to calculate the log P value of each matrix compound.

Solubility of matrix compounds

An experimental study was designed for a direct comparison of the five matrix compounds. The study was designed to maintain same 0.2 M matrix concentration,

solubilized in the same solvent, and contained the same amount of 0.04 M ammonium citrate dibasic. The only variable component was the matrix compounds. The solubility of the five matrix compounds were investigated in either 1 mL of 50% ACN or 50% DMF to obtain a target concentration of 0.2 M matrix solution. For comparing the use of two solvents (50% ACN or 50% DMF), 0.2 M matrix solutions were prepared for each matrix compound. MALDI matrix compounds were dissolved in 50% ACN or 50% DMF, both containing 0.04 M ammonium citrate dibasic, and determined maximum solubility of each matrix compound. The amount of matrix solubilized in each of the solvents was recorded. The results were compared to determine which was the best solvent, which yielded matrix concentrations nearest to 0.2 M.

Drying time for selected matrix compounds

A drying study was performed to determine the drying time of 0.3 µL droplet of each matrix solution that were prepared in 50% DMF and 0.04 M ammonium citrate dibasic solution. 0.3 µL droplets of each matrix solution were spotted on MALDI sample plate, allowed to air dry and the drying times were recorded.

UV absorbance of selected matrix compounds

Matrix solutions were prepared by dissolving 2.5 g of each matrix compound into 1 mL of 10% ACN that contained 0.04 M ammonium citrate dibasic. 1.0×10^{-5} M matrix solutions were obtained through serial dilutions of each of matrix solution for UV absorbance measurements. A Varian 50Bio Ultra Violet-Visible spectrophotometer

equipped with a quartz cuvette was used to acquire absorbance scan of each matrix solution. 10% ACN that contained 0.04 M ammonium citrate dibasic solution was used as the blank. The parameters for absorbance scans were set accordingly; X mode: 600 nm to 200 nm, Y mode: Abs and dual beam mode. The scan controls were set to an average time of 0.0125 s, data interval of 0.20 nm and scan rate of 960.00 nm/min with baseline correction. The extinction coefficient of each matrix was determined using the Beer's-Lambert Law and absorbance values at 355 nm.

Preparation of MALDI samples

All matrix compounds (3-HPA, THAP, DABP, 6-ATT, 3-HC) were dissolved in 50% DMF containing 0.2 M matrix and 0.04 M ammonium citrate dibasic, 0.3 µL droplets were spotted on MALDI sample plate. Microscopic image of each spot was acquired by using a digital eyepiece camera mounted on an inverted microscope and equipped with an external light box to enhance visual clarity. Visual images of thin-layer matrix spots and thin-layer matrix spots loaded with 0.3 µL droplets of 20 µM miR-124a sample were compared to observe the changes on each sample.

"Spiking" experiment with 3-HPA matrix

A stock solution of 0.25 M 3-HPA matrix, 0.04 M ammonium citrate dibasic was prepared in 10% ACN. A diluent solution containing 0.04 M ammonium citrate dibasic was also prepared in 10% ACN. Starting with 0.25 M 3-HPA stock solution, stock solution was diluted with the diluent to obtain solutions containing 125,000 – 1953 µM 3-

HPA matrix. A stock solution of 100 μM miR-124a was used to prepare each "spiking" sample. Equal volume of each diluted 3-HPA matrix solution was added to an equal volume of 100 μM miR-124a, to yield 50 μM miR-124a "spiked" samples. The "spiked" samples are quickly spotted in 0.3 μL droplets onto MALDI sample plate for MALDI-TOF MS analysis.

CHAPTER III

RESULTS AND DISCUSSION

The use of MALDI mass spectrometry to measure DNA has been more popular than RNA. Thus, there are limited number of reports on the topic of MALDI mass spectrometry of RNA, and even less for the analysis of miRNA. In general, the basic molecular structures of DNA and RNA are similar to each other. However, the 2'-hydroxyl group in each ribonucleotide has induced the formation of many unique secondary structures in different RNA molecules as well as changing the reactivity of RNA towards many chemical reactions. For these reasons, the analytical performance of MALDI mass spectrometry of RNA is not expected to be identical as in the case of measuring DNA. Based on the previous experience in our research group on using MALDI-TOF MS to measure DNA[11], the most commonly used 3-HPA matrix could generate relatively strong signals from measuring small DNA oligos. For the purpose of carrying out the subsequent MS/MS measurements of miRNA, relative high signal intensity in linear MALDI-TOF MS measurements is required. This is because if more precursor miRNA ions will be available for undergoing the CID process, more fragment ions will be generated. Thus, the use of 3-HPA matrix in linear MALDI-TOF MS was examined at the beginning of this study. In an initial experiment, the standard 0.25 M 3-HPA matrix, 0.04 M ammonium citrate dibasic and 20 μM miR-124a sample were spotted on the sample plate by using the thin-layer method, and analyzed with linear

positive mode in MALDI-TOF MS. The peak that corresponded to $[\text{miR-124a} + H^+]^+$ (7161.3 *m/z*) was detected as shown in Figure 2, along with peak that corresponded to $[\text{miR-124a} + 2H^+]^{2+}$ (3581.1 *m/z*). The singly-charged $[\text{miR-124a} + H^+]^+$ ion was detected at 7161.3 *m/z* due to the transfer of a proton (H^+) from 3-HPA matrix to ionize miR-124a during the MALDI desorption/ionization process. The doubly-charged $[\text{miR-124a} + 2H^+]^{2+}$ ion was generated by transferring $2H^+$ from 3-HPA, and yielded a m/z value of 3581.1. Na^+ adduct peaks were also observed on the right-hand side of the singly and doubly-charged ion peaks, adding an additional 22 Da to $[\text{miR-124a} + H^+]^+$ and 11 Da to $[\text{miR-124a} + 2H^+]^{2+}$. 3-HPA matrix cluster ions were found at below 300 *m/z* (not shown), therefore did not interfere with the MALDI-TOF MS measurements of miR-124a precursor ions as observed in Figure 2, and allowing the correct selection of miR-124a precursor ions for MS/MS measurements.

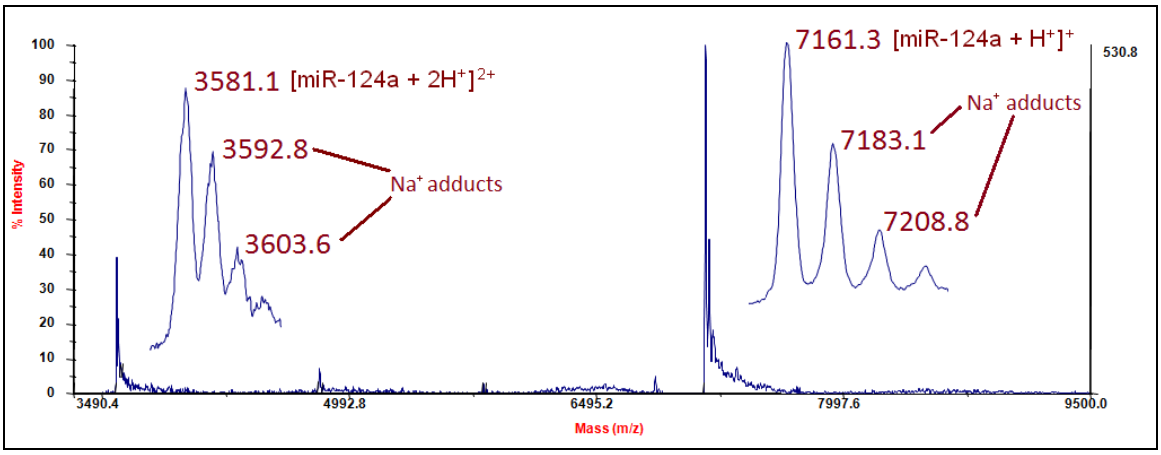

Figure 2. MALDI mass spectrum of 20 µM miR-124a. The theoretical mass of a singly-charged $[\text{miR-124a} + H^+]^+$ ion is 7161.3 Da.

In 2006, Andersen and co-workers[12] have studied the collision-induced dissociation of 4-mer RNA fragments by using tandem MALDI-TOF/TOF MS, and proposed a mechanism for the collision-induced dissociation of RNA molecule, in which the presence of a 2'-hydroxyl group in each ribonucleotide has favored the formation of c- and y-ions in comparison to (a-B)- and w-ions as in the case of DNA fragmentation.

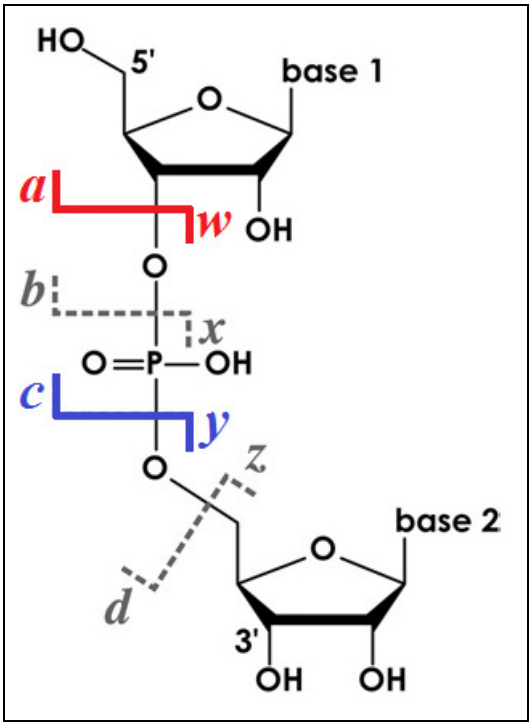

Figure 3. Schematic of possible fragmentation sites on RNA oligonucleotide structure. c-y fragmentation is more favorable during RNA fragmentation.

More recently, by using the technology of ion trap, McLuckey[19] and his associates have confirmed the 2'-OH group on RNA significantly facilitates the production of c/y-ions. In order to minimize the base loss and internal fragmentation of RNA precursor ions, Breuker and her associates[20] have adopted the use of collisional cooling of precursor ions and the selection of precursor ions of relatively low negative net charge. In the case

of MALDI mass spectrometry, majority of precursor ions are singly charged as shown in Figure 2. In comparison to molecular ions that carry multiple charges, the internal energy of singly charged ions are expected to be considerably lower. For this reason, both base loss and internal fragmentation of precursor ion of miR-124a were not observed. On the other hand, high CID energy (≥ 1 KeV) can be achieved when the molecular ions are extracted into the time-of-flight mass analyzer by using a potential difference as high as 20 kilovolt. As demonstrated in a recent paper from our research group, the high CID energy in tandem MALDI-TOF/TOF MS measurements of DNA adducts had induced more fragmentation of the precursor ion than using other MS/MS techniques. In summary, MALDI-TOF/TOF MS has the advantage on minimizing base loss and internal fragmentation of RNA precursor ions at the initial stage of desorption/ionization process, and provides relatively high CID energy to induce RNA fragmentation in MS/MS measurements. For these reasons, all experimental work in this thesis has focused on using MALDI-TOF/TOF as the primary MS technique.

For initial MS/MS measurements, the singly charged [miR-124a + H^+]$^+$ ion was selected as precursor ion, because of its higher ion count and S/N ratio in comparison to the doubly-charged [miR-124a + $2H^+$]$^{2+}$ ion. The 7161.3 *m/z* peak was first identified in the linear mode. The [miR-124a + H^+]$^+$ ion was selected by using a timed ion selector with a mass window of ±10 Da of the focus mass of the selected precursor ion. Precursor ions were channeled through a collision cell at 10^{-7} Torr, where ions were bombard with atmospheric gas molecules and underwent fragmentation. The fragment ions were then extracted into the second TOF analyzer where the ions were separated. An initial

MS/MS spectra of 25 µM miR-124a was generated (Figure 4) providing peaks identifiable as precursor ions. In Figure 4, the S/N ratio of the precursor ion was lower than expected partly due to the background noise level was relatively high. There might be potential CID fragments in the MS/MS measurements, but signals were too low to be detected.

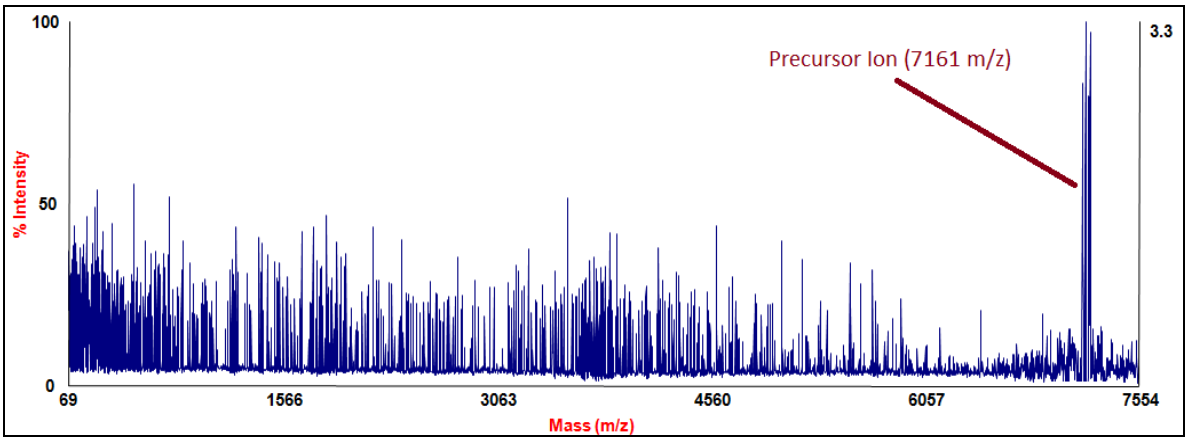

Figure 4. Initial MS/MS spectrum of 25 µM miR-124a. Focus mass of 7161 *m/z*, mass window: ± 10 Da.

In order to improve the signal intensity of each CID fragment, more precursor ions must undergo the CID process. One of the approaches to ensure an increase on the number of precursor ions would be available for the CID process is to optimize the initial MALDI process. Therefore, most of the remaining efforts in this research thesis focused on optimizing the desorption of RNA during the MALDI process.

Effects of laser intensity on measuring 3-HPA matrix

The protonated 3-HPA ion corresponded to 140.2 *m/z* peak in the spectrum Figure 5a, along with peaks that corresponded to various matrix cluster ions. We investigated MALDI process of 3-HPA matrix with increasing laser intensity from 5,000 – 7,900 arb. units to determine the optimal laser intensity to produce the highest amount of 3-HPA ion to support the desorption/ionization of selected miRNA analyte. In Figure 5b, the ion count for the 3-HPA ion is at the lowest level when laser intensity of 5,000 – 6,000 arb. units were used. The highest signal of 3-HPA was obtained with laser intensity of 7,000 – 7,900 arb. units. From this investigation, we determined that the optimal laser intensity for producing maximum number of 3-HPA ions is between 7,000 – 7,500 arb. units of laser intensity.

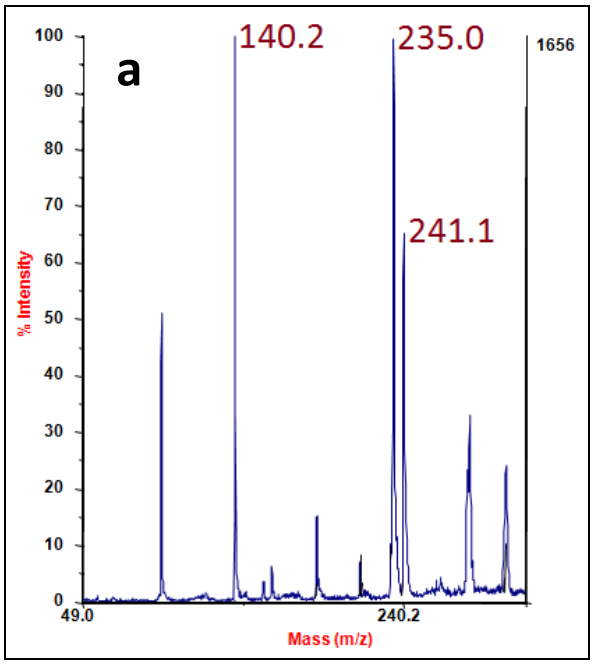

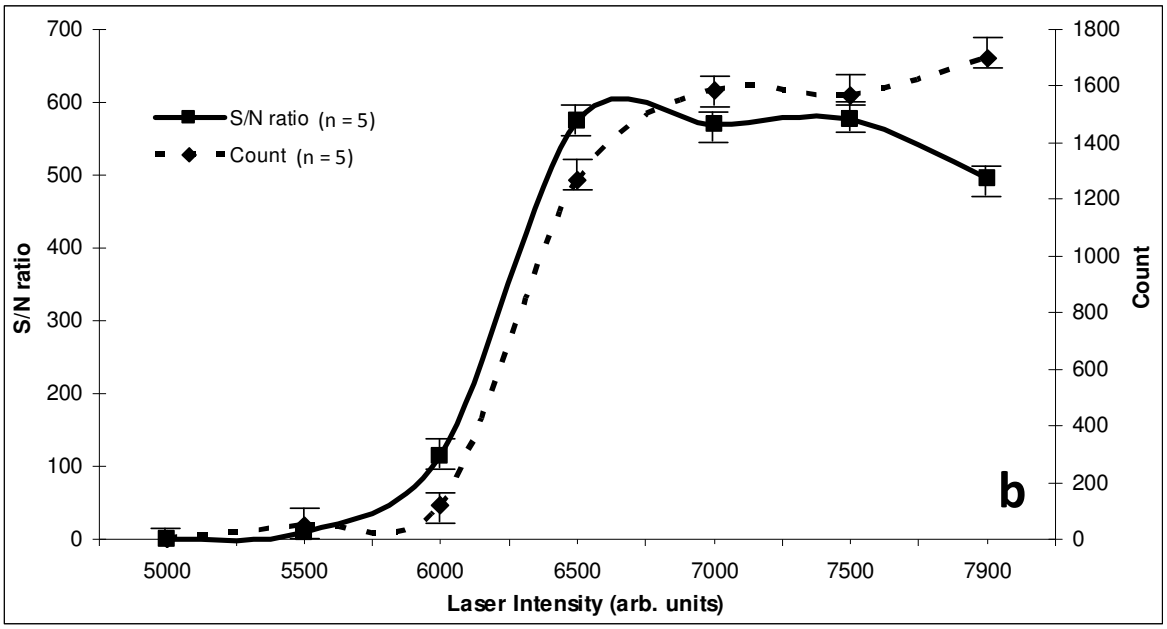

Figure 5. (a) MALDI mass spectrum of 3-HPA matrix, and (b) effects of laser intensity on signal-to-noise (S/N) ratio and ion count of 3-HPA matrix ion.

Effects of laser intensity on measuring miR-124a

3-HPA matrix and its cluster ions are shown in the MALDI-TOF linear MS spectrum below (Figure 6a), along with the $[\text{miR-124a} + H^+]^+$ ion species at 7161.9 *m/z*. From Fig 6a, the 3-HPA matrix ion peak is at the lower mass range as compared to the peak of $[\text{miR-124a} + H^+]^+$ ion. The spectral resolution in Figure 6a can allow accurate identification of miR-124a and eliminates any chance of matrix interference. We investigated the effects of increasing the laser intensity (5,000 – 7,900 arb. units) on S/N ratio and ion count of $[\text{miR-124a} + H^+]^+$ ion by using the linear positive ion mode in MALDI-TOF MS. The S/N ratio and ion count of miR-124a signal were below the detectable level as shown in Figure 6b. At laser intensity of 6,000 – 7,000 arb. units, there was minimal detection of $[\text{miR-124a} + H^+]^+$ ion. The highest signal intensity was observed at laser intensity of 7,500 arb. units, while the signals began to drop at the maximum level of laser intensity. The optimal S/N ratio and ion count for $[\text{miR-124a} + H^+]^+$ ion occurs at laser intensity 7500 and correlates with the investigation of using different laser intensity to desorb and ionize 3-HPA matrix.

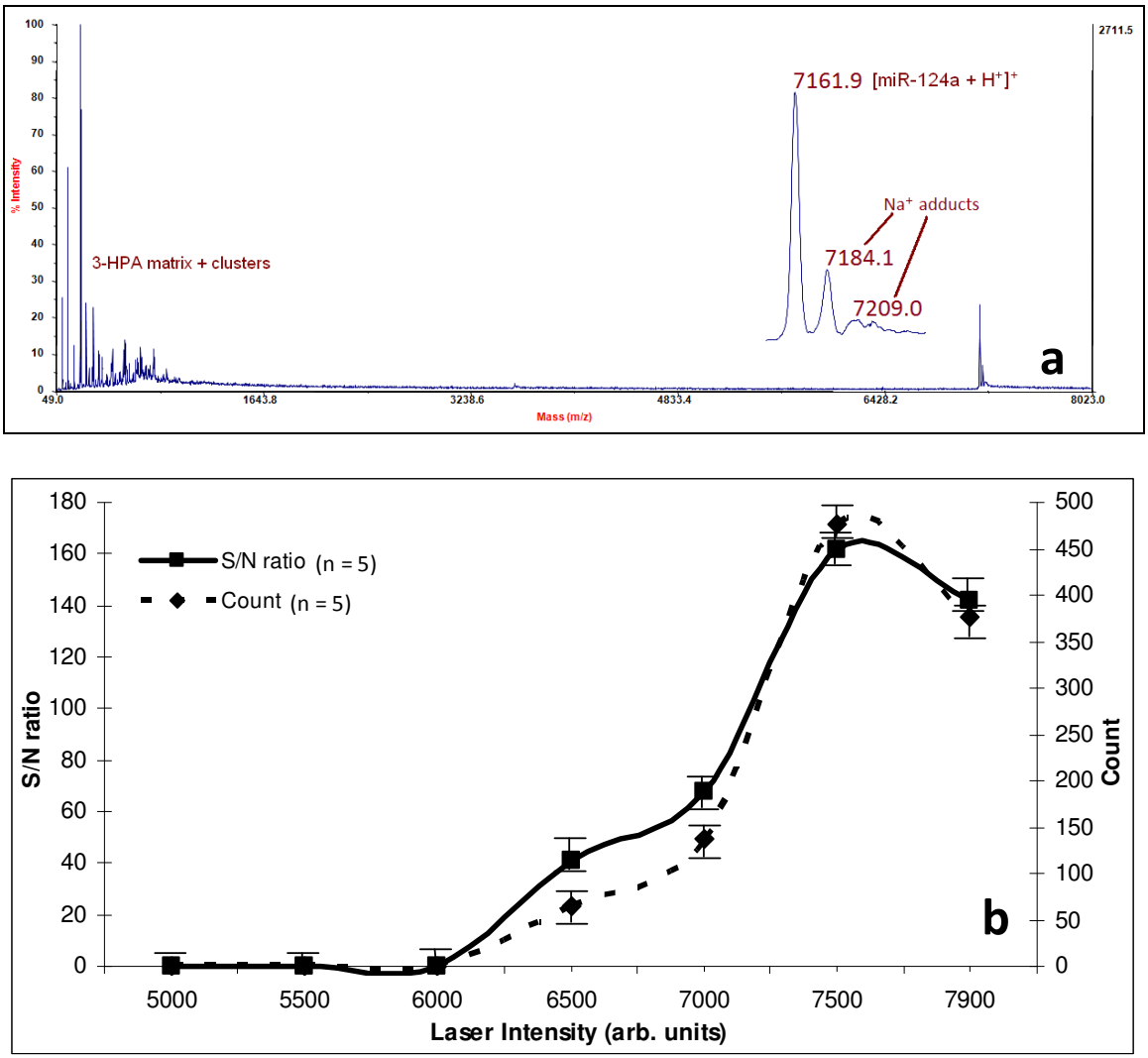

Figure 6. (a) MALDI mass spectrum of 20 µM miR-124a, and (b) effects of laser intensity on signal-to-noise (S/N) ratio and ion count of $[\text{miR-124a} + H^+]^+$ ion.

Effects of increasing miR-124a concentration

Besides optimizing the laser intensity, another approach to increase to the signal intensity in any instrumental technique including MALDI mass spectrometry is to increase the concentration of analyte being measured. Thus, the effects of increasing the concentration of miR-124a to the MALDI-TOF MS measurements of miR-124a were investigated by using the optimal laser intensity. MALDI spectra were acquired by using various miR-124a concentrations as shown in Figure 7a. Surprisingly, the signals of $[\text{miR-124a} + H^+]^+$ ion at 7,161 m/z were decreased after reaching the maximum level around 10 μM (Figure 7b). By comparing the spectra with increasing miR-124a concentration, there is a noticeable increase in the peak intensity of Na^+ adducts, i.e. miR-124a + Na^+ ion. This was due to the fact that the miR-124a standard was not absolutely free of sodium salt and the amount of ammonium ions in the matrix solution for suppressing Na^+ adduct was fixed. Thus, with an increasing amount of miR-124a sample, more Na^+ adducts were observed when the sample was measured by using MALDI-TOF MS. More importantly, this has lowered the signal intensity that corresponded to the $[\text{miR-124a} + H^+]^+$ ion as shown in Figure 7b. Since the Na^+ adducts would normally be excluded from the subsequent MS/MS measurements, the use of increasing concentration of miR-124a in the MALDI sample would not be beneficial. From Figure 7b, the optimal range of miR-124a concentration is 5 – 20 μM, with 10 μM yielding the maximum S/N ratio and ion count.

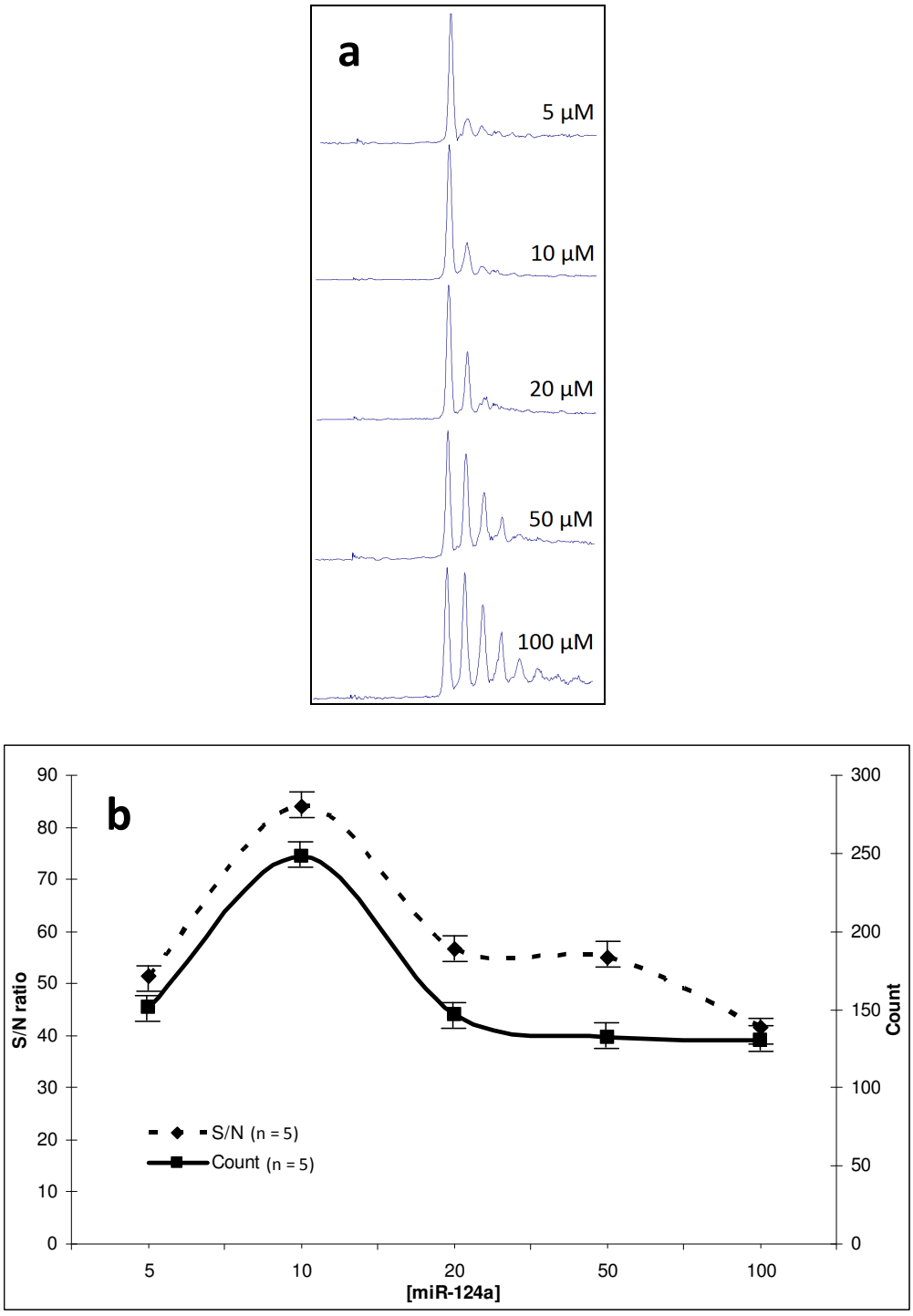

Figure 7. (a) MALDI mass spectra of miR-124a at different concentrations, and (b) effects of miRNA concentration on its corresponding signal-to-noise (S/N) ratio and ion count in MALDI-TOF MS measurements.

Thin-layer versus dried droplet method

To determine which sample preparation method would provide better mass resolution, and S/N ratio for measuring miR-124a, two different MALDI sample preparation methods were compared. From the mass spectrum that was obtained by using the thin-layer method (Figure 7a), minimal noise interference was observed and yielded strong signals for both [miR-124a + H^+]$^+$ and [miR-124a + $2H^+$]$^{2+}$ ions. Whereas, the results obtained from using the dried droplet method (Figure 7b) have shown an increase in noise interference and only yielded a lower signal for [miR-124a + H^+]$^+$ ion. The comparison of mass resolution and S/N ratio confirm that thin-layer sample preparation method yields higher signal intensity. Premixing the RNA sample with 3-HPA matrix solution in the dried droplet method might lead to different rate of co-crystallization of 3-HPA matrix with the RNA sample and resulting in less favorable crystal morphology, thus yielding a lower signal for miR-124a.

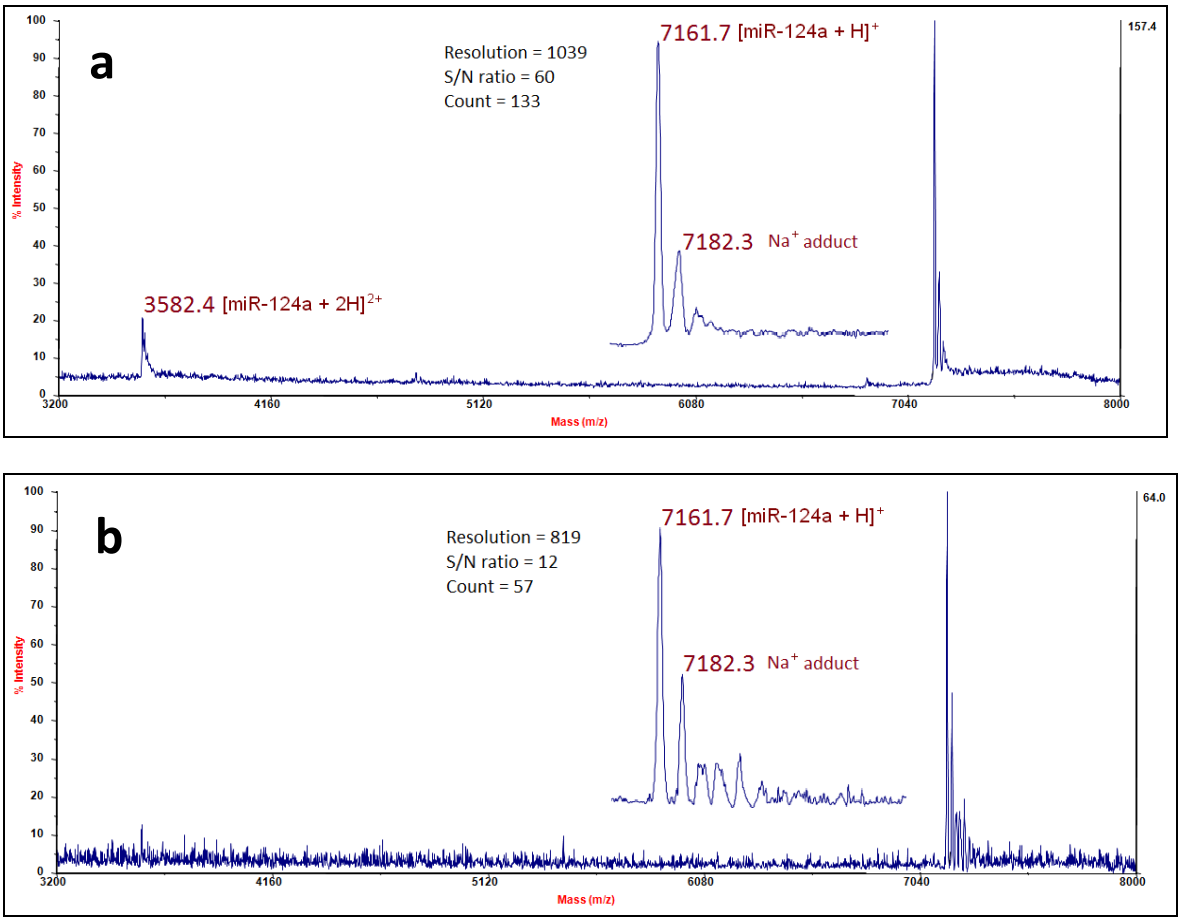

Figure 8. MALDI mass spectra of 20 μM miR-124a samples that were prepared by using (a) thin-layer method and (b) dried droplet method.

Hydrophobicity of matrix compounds

Hydrophobicity can be considered as a measure of how insoluble a chemical compound is in water or polar solvent. In Table 2, the 3-D molecular structure of each matrix compound is illustrated. To evaluate the hydrophobicity of the selected MALDI matrix compounds, the log P value of each matrix compound was calculated. By definition, P is the partition coefficient of a compound between two solutions, which is equivalent to the ratio of concentrations of the compound between the two solutions. The

calculations of all log P values were carried out by using the ACDlabs 12.0 ChemSketch software. A low log P value represents the compound is less hydrophobic or more soluble in water as well as weaker intermolecular interaction. Whereas, a high log P value represents the compound is more hydrophobic or less soluble in water as well as stronger intermolecular interaction. The log P values for 3-HPA (0.72 ± 0.36) and 6-ATT (-0.42 ± 0.83, -1.46 ± 0.64) were lower than the other three matrix compounds, indicating 3-HPA and 6-ATT are most likely to be dissolved in polar solvents. 6-ATT contains two different log P values due to its ability to exist in two different states of electronic localization, transferring electrons from oxygen to sulfur atom. THAP, 3-HC and DABP have comparatively high log P values, thus these compounds are expected to be less soluble in polar solvents. Based on their log P values, the hydrophobicity of the selected matrix compounds can be ranked in the following order: 6-ATT < 3-HPA < 3-HC < THAP < DABP. As shown in Table 2, all five selected matrix compounds have shared similar aromatic ring structure. Thus, their order of hydrophobicity is comparable to the increasing order of their molecular masses. In other words, for the selected MALDI matrices, the hydrophobicity of the matrix compound is proportional to its molecular mass.

Table 2. 3-D structure and Log P value of matrix compounds

Matrix Compound	3-D Structure	Mass (g/mol)	Log P Value
3-hydroxy picolinic acid (3-HPA)	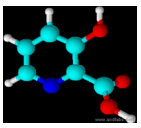	139.11	0.72 +/- 0.37
2',3',4'-trihydroxyacetophenone (THAP)	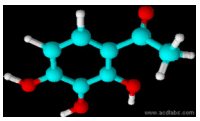	168.15	1.73 +/- 0.37
3,4-diaminobenzophenone (DABP)	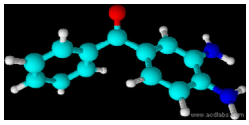	212.25	2.19 +/- 0.43
3-hydroxycoumarin (3-HC)	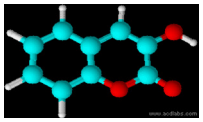	162.14	1.60 +/- 0.76
6-aza-2-thiothymine (6-ATT)	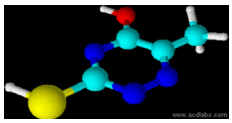	143.17	-0.42 +/- 0.84 -1.46 +/- 0.65

Solubility of selected matrix compounds

Based on an in-depth literature study of the recent publications in which MALDI mass spectrometry was used to measure either DNA or RNA, the most commonly used MALDI matrix concentrations were between 0.1 M and 0.2 M. For the purpose of comparing the outcomes of using each individual matrix compound to measure miRNA, the same matrix concentration must be used. Thus, the concentration of 0.2 M was chosen as a reference point in this study. The reason for choosing a higher matrix concentration was to ensure the ratio of matrix to analyte in the final co-crystalline sample was as high as possible, which is one of the general requirements for successful MALDI mass spectroscopic measurements. In other words, excessive matrix is needed to support the MALDI process. The amount of matrix required to prepare 1 mL of 0.2 M

matrix solution was determined for each of the five matrix compounds (Table 3). Using these values as reference, saturated matrix solutions were prepared for each of the matrix compounds using 50% ACN. It was determined that 3-HPA was readily dissolved and reached 0.25 M. Whereas, THAP, DABP and 6-ATT were less soluble and yielded concentrations of < 0.1 M. For 3-HC, it was practically insoluble in 50% ACN. Since 0.2 M matrix solution was not achievable for 4 out of 5 matrix compounds, an alternative solvent was selected (50% DMF). All five matrix compounds were readily dissolved in 50% DMF, and 0.2 M of each individual matrix solution was prepared. The reason for using only 50% DMF instead of 100% DMF was because 0.04 M of ammonium citrate dibasic was a required component in the matrix solution, which would not be soluble in 100% DMF. Normally, ammonium citrate dibasic is served as a desalting reagent in MALDI matrix, and is essential to MALDI mass spectrometry of nucleic acids.

Table 3. Solubility of matrix compounds in 50% ACN:H_2O and 50% DMF:H_2O

		50% ACN:H_2O		50% DMF:H_2O	
Matrix	Amount (mg) [0.2 M]	Amount Dissolved (mg)	Conc. (M)	Amount Dissolved (mg)	Conc. (M)
3-HPA	27.82	35.0	0.25	27.8	0.20
THAP	33.63	10.2	0.06	33.6	0.20
DABP	42.45	2.2	0.01	47.3	0.22
3-HC	32.43	-	-	32.5	0.20
6-ATT	28.63	11.8	0.08	28.3	0.20

Drying time of selected matrix compounds

It has been reported that the rate of drying the matrix-sample mixture on the MALDI sample plate is related to the outcome of MALDI mass spectroscopic measurements. For this reason, one of the initial experiments in this study was to determine the drying time for selected matrix solutions. In addition, it would become impractical to wait for a long time to dry a matrix-sample mixture before a measurement could be carried out. In Table 4, all the drying time for 0.3 µL droplet of each matrix solution were recorded. 3-HPA matrix droplet was completely dried after 5 minutes at room temperature and pressure. This was followed by 6-ATT at 10 minutes and 3-HC at 20 minutes. Both THAP and DABP matrix droplets were dried after one hour and more than two hours waiting, respectively. Comparison of ascending drying time, the matrix compounds prepared in 50% DMF can be ranked in the following order: 3-HPA < 6-ATT < 3-HC < THAP < DABP. Ideally, the drying time for a matrix droplet should not take longer than 5 minutes. The prolonging of drying time can potentially jeopardize the matrix itself because MALDI matrix compounds are sensitive to light. The drying time of the sample droplet must also be considered. This is because the addition of the sample to the matrix solution will also extend the amount of time for drying the mixture before the measurement can be carried out. Since other solvents, for example DMSO, might not be fully compatible with MALDI mass spectrometry, 50% DMF was considered to be the best solvent for dissolving the selected matrix compounds in this study.

Table 4. Drying time of 0.2 M matrix solutions prepared in 1 mL 50% DMF:H_2O solvent

Matrix Compound	Matrix (mg) in 1 mL [0.2 M]	Matrix (ug) in 0.3 uL	Drying Time (minutes)
3-HPA	27.8	8.34	5
THAP	33.7	10.11	60
DABP	42.5	12.75	>2 hrs
3-HC	32.5	9.75	20
6-ATT	28.6	8.58	10

UV absorbance of selected matrix compounds

In order to determine which is the most important property of the selected matrix compounds for supporting the MALDI process, i.e. generation of molecular analyte ions, the UV absorbance of each matrix compound was measured. To facilitate the MALDI process, the 4700 Applied Biosystems Proteomics analyzer that has been used in this study is equipped with a 355 nm Nd:YAG laser. Other MALDI-TOF mass spectrometers may use a different source of laser, for example nitrogen laser (335 nm). Therefore, instead of single wavelength measurements, UV scan of each matrix compound was performed. The UV scans would also allow us to correlate the UV absorbance at 355 nm of each matrix compound to the production of both 3-HPA and miRNA molecular ions. In Figure 9, when comparing the absorbance at 355 nm, the higher absorbance of DABP at is due to the fact that higher concentration of DABP was used. Otherwise, THAP and 3-HC have comparable absorbance at 355 nm, and both 3-HPA and 6-ATT are undetectable. This was due to the fact that all UV absorbance measurements had to be carried out at much lower concentrations than they were normally used in MALDI sample preparation. Nevertheless, the results in Figure 9 do allow us to compare the absorptivity of selected matrix compounds for UV photons being used in the MALDI

process. By using the Beer's-Lambert law, the extinction coefficient of selected matrix compounds at 355 nm were calculated (Table 5). In general, the higher the extinction coefficient, the higher the efficiency on absorbing the photon. The extinction coefficients were not calculated for 3-HPA and 6-ATT because their absorbance at 355 nm were undetectable.

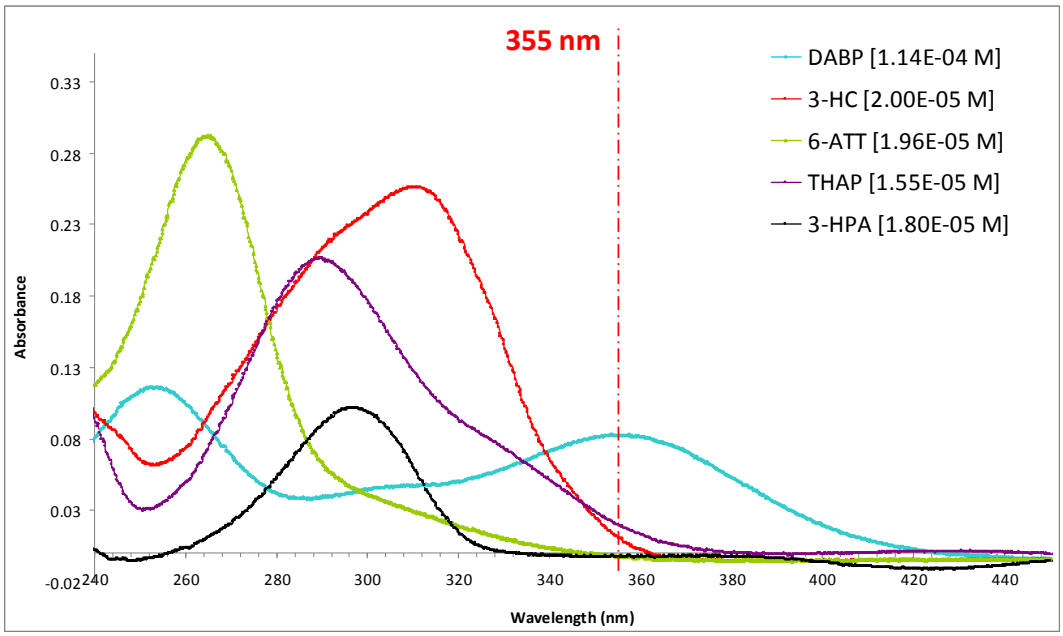

Figure 9. UV absorption spectra (200-600nm) of five different matrix compounds prepared in 10% ACN:H_2O and 0.04 M ammonium citrate dibasic solution.

Table 5. Extinction coefficient of matrices at 355 nm wavelength

Matrix Compound	Concentration (M)	Absorbance at 355 nm	Extinction Coefficient (cm^{-1} L mol^{-1})
3-HPA	1.80E-05	-	-
THAP	1.55E-05	0.0201	1297
DABP	1.14E-05	0.0826	7246
3-HC	2.00E-05	0.0107	535
6-ATT	1.96E-05	-	-

Co-crystallization of MALDI matrix with miR-124a

Microscopic images of matrix spots and spots that contained both matrix and miR-124a were recorded in Table 6. By comparing the images of matrix spots, it is obvious the physical and chemical properties of selected matrix compounds including their hydrophobicities are different from each other. Therefore, the physical appearance of these images could indirectly confirm the calculations of log P values are reliable. The appearance of 3-HPA, THAP, and DABP were significantly changed after the matrix was redissolved and co-crytallized with miR-124a. Whereas, the physical appearance of 3-HC and 6-ATT did not change much following the co-crystallization with miR-124a. As documented in the literature by several other research groups, the co-crystallization process between MALDI matrix and analyte of interest is important to the success of MALDI mass spectroscopic measurements. This is because the intermolecular interactions between MALDI matrix and analyte of interest within the matrix-sample co-crystalline sample could directly affect the extent of matrix protection for the more fragile analyte molecules from laser irradiation as well as the subsequent desorption of analyte from the co-crystalline sample. Another important observation that could be made from the images of the spots that contained both matrix and miR-124a was the distribution of co-crystals was uneven. For example, in the case of 3-HPA, the co-crystals clustered around the edge of the spot. This information would be useful for searching the areas in which stronger signals could be obtained from the co-crystalline sample. From Table 6, it has also been noted DABP and 6-ATT spots did not have uniform crystalline structure. In the case of DABP, it might be the cause of negative

results from MALDI mass spectroscopic measurements (see below). The uniformity in co-crystalline structure is expected to allow for better matrix-analyte interactions. This study was based on physical observations only, therefore to confirm if crystal formation plays an important role in MALDI-MS measurements of miR-124a, MALDI-TOF MS analysis was required.

Table 6. Photograph of dried matrix spots prepared in 50% DMF:H_2O

Matrix Compound	Matrix only	Loaded with sample
3-hydroxy picolinic acid (3-HPA)		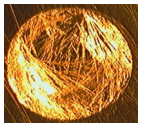
2',3',4'-trihydroxyacetophenone (THAP)		
3,4-diaminobenzophenone (DABP)		
3-hydroxycoumarin (3-HC)		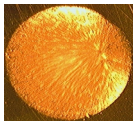
6-aza-2-thiothymine (6-ATT)	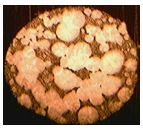	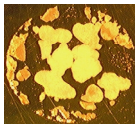

MALDI-TOF MS analysis of miR-124a spotted on 3-HC and DABP matrix did not yield any signal that corresponded to $[miR\text{-}124a + H^+]^+$ ions. Whereas, the use of 6-ATT, THAP, or 3-HPA matrix all yielded detectable amount of $[miR\text{-}124a + H^+]^+$ ions as

shown in Figure 10. From the spectra of using 6-ATT and THAP as matrix, relative low S/N ratios were obtained from the detection of miR-124a. In the case of 3-HPA, the highest S/N ratio for $[miR\text{-}124a + H^+]^+$ ions was achieved. Overall, MALDI-TOF MS analysis confirmed 3-HPA matrix as the best matrix to be used for miR-124a analysis.

"Spiking" experiment with 3-HPA matrix

After comparing the outcome from using the selected matrix compounds in the previous section, it was confirmed that 3-HPA matrix could generate the highest signals for MALDI-TOF mass spectrometry of miRNA. A further investigation was conducted to optimize the use of 3-HPA matrix by using a modified sample preparation method referred as "spiking". This study was designed to determine if additional levels of 3-HPA matrix spiked into miR-124a sample would help to increase S/N ratio and ion count of $[miR\text{-}124a + H^+]^+$ ion. By using the conventional thin-layer sample preparation method i.e. no additional 3-HPA matrix, S/N ratio of 17 and ion count of 68 were obtained from measuring 50 μM of miR-124a. As shown in Table 7, as the amount of additional 3-HPA was increased in this experiment, both S/N ratio and ion count of $[miR\text{-}124a + H^+]^+$ ion were increased. At the highest level (50%) of additional 3-HPA, the S/N ratio was increased more than 4 times in comparison to the conventional sample preparation method. The significant increase on S/N ratio confirms that "spiking" the miR-124a sample with additional 3-HPA matrix before spotting on a thin-layer of dried

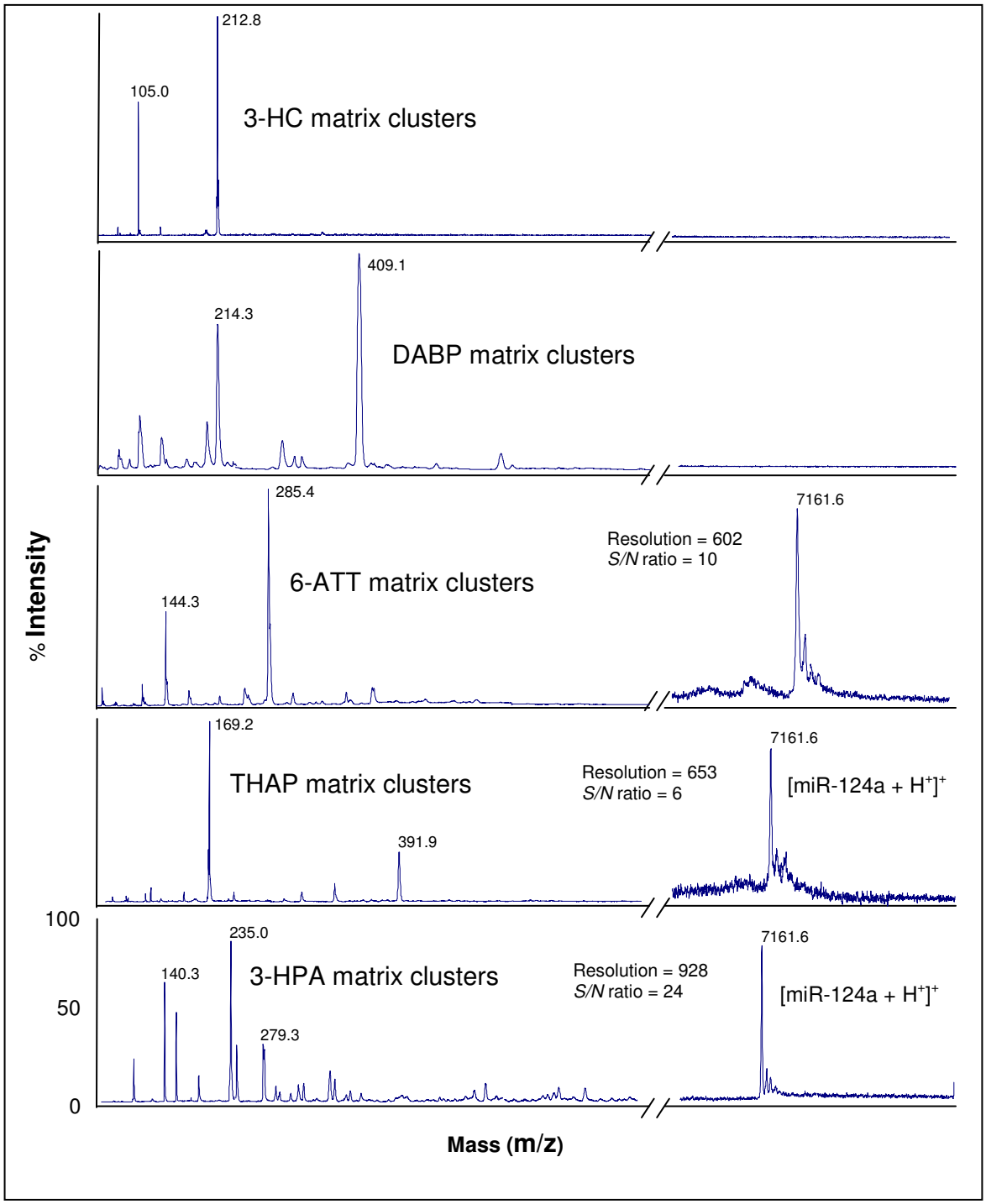

Figure 10. MALDI mass spectra of 5 μM miR-124a samples that were prepared by using the thin-layer method and different matrix compounds.

3-HPA matrix help to acquire stronger MALDI MS signals. One of the key factors that caused an increase on the signals was due to the presence of additional ammonium citrate dibasic in the 3-HPA matrix, which further eliminated the sodium adducts of miR-124a and increased the signal of $[\text{miR-124a} + H^+]^+$ ion. This was confirmed by the data obtained from adding 0 μM 3-HPA to 50 μM miR-124a sample, which yielded a S/N ratio of 45 (Table 7). Based on the results in Table 7, the modified sample preparation method, which involves spiking a sample of interest with additional MALDI matrix before adding the mixture of matrix and sample on top of a spot of dried matrix, has a great potential to expand the current linear dynamic range for quantitation in MALDI mass spectrometry of different analytes.

Table 7. Summary of 3-HPA "spiking" study to optimize *S/N* ratio

[3-HPA matrix]	% 3-HPA matrix Conc. Increase	[miR-124a]	S/N	miR-124a Resolution	Count
125000 μM 3-HPA	50.0%	50 μM miR-124a	80	801	360
62500 μM 3-HPA	25.0%	50 μM miR-124a	55	876	194
31250 μM 3-HPA	12.5%	50 μM miR-124a	49	961	230
15625 μM 3-HPA	6.3%	50 μM miR-124a	41	915	152
7813 μM 3-HPA	3.1%	50 μM miR-124a	40	1003	164
3906 μM 3-HPA	1.6%	50 μM miR-124a	43	962	154
1953 μM 3-HPA	0.8%	50 μM miR-124a	44	953	186
125000 μM 3-HPA	50.0%	0 μM miR-124a	-	-	-
0 μM 3-HPA	0.0%	50 μM miR-124a	45	1009	179
250000 μM 3-HPA	-	50 μM miR-124a	17	927	68

Investigation of MALDI-TOF MS/MS parameters

With the optimal parameters that have been determined to acquire maximum S/N ratio and ion count in the linear mode of MALDI-TOF MS, the focus of our efforts is shifted back to the MALDI-TOF MS/MS measurements of selected miRNA model.

Initially, the results from using the positive and negative ion mode to acquire the MS/MS spectra were compared. As shown in Figure 11, the precursor ion of miR-124a was detected in the positive ion mode, and not detectable in the negative ion mode. None of the expected CID fragments of miR-124a was detectable in both spectra. Nevertheless, it was concluded the positive ion mode would be our choice to further the MS/MS experiments in this study.

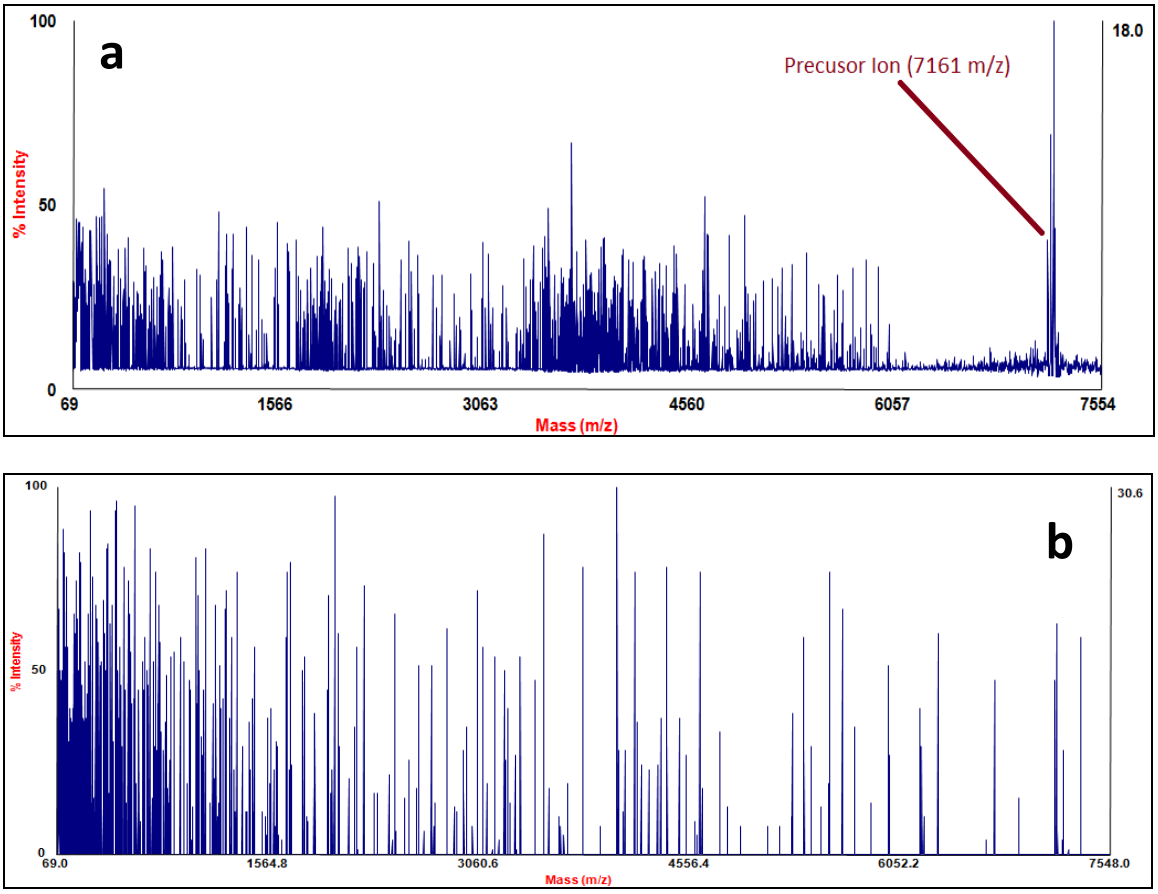

Figure 11. MS/MS spectra of $[miR\text{-}124a + H^+]^+$ at (a) positive and (b) negative ion mode. 20 µM miR-124a was spotted on 3-HPA thin-layer matrix and analyzed using laser intensity = 7500 arb. units, CID pressure = $1.0e^{-08}$ Torr and delay time = 68321 ns.

In order to ensure there would be sufficient collisional gas to induce the fragmentation of miR-124a, the effects of different pressure of atmospheric air inside the collision cell were investigated. An increase on the CID pressure may lead to additional collisions between air particles and miR-124a precursor ions, thus generating more CID fragments. Referring to the results in Figure 12, low CID pressure at $1.0e^{-07}$ Torr and $5.0e^{-07}$ Torr did not produce sufficient CID fragments for partial *de novo* sequencing. Whereas, with increasing CID pressures ($\geq 1.0e^{-06}$ Torr), some of the CID fragments of miR-124a became detectable. For more in-depth spectral interpretation of MS/MS spectra, please refer to the last section of this Chapter. Overall, the increase on CID pressure did induce the fragmentation of miR-124a precursor ion (7,161 m/z) which would usually considered to be technically challenging for MALDI-TOF MS/MS.

The manual setting of delay time for Source 2 in MALDI-TOF/TOF MS can be considered as a control for the duration of CID process before any fragment ions are extracted into the second TOF mass analyzer. With longer the duration of CID process, there would have been more time to induce the fragmentation of precursor ion. Owing to this reason, the effects of different duration of CID process (or delay time in Source 2) were investigated. With delay time between 20,000 and 50,000 ns, only minimal CID fragments were detected as shown in Figure 13a. These delay times might not provide sufficient time for the CID process to induce the fragmentation of selected precursor ion before any CID fragments were extracted from the CID cell or Source 2. With delay time longer than 65,000 ns, similar MS/MS spectral patterns (Figure 13b) were observed as in the study of CID pressure. The delay time of 68,000 ns is considered to the optimal delay

time for the fragmentation of miR-124a precursor ion. This was partly because some of the remaining precursor ion was detected which was very useful for recalibrating the MS/MS spectrum.

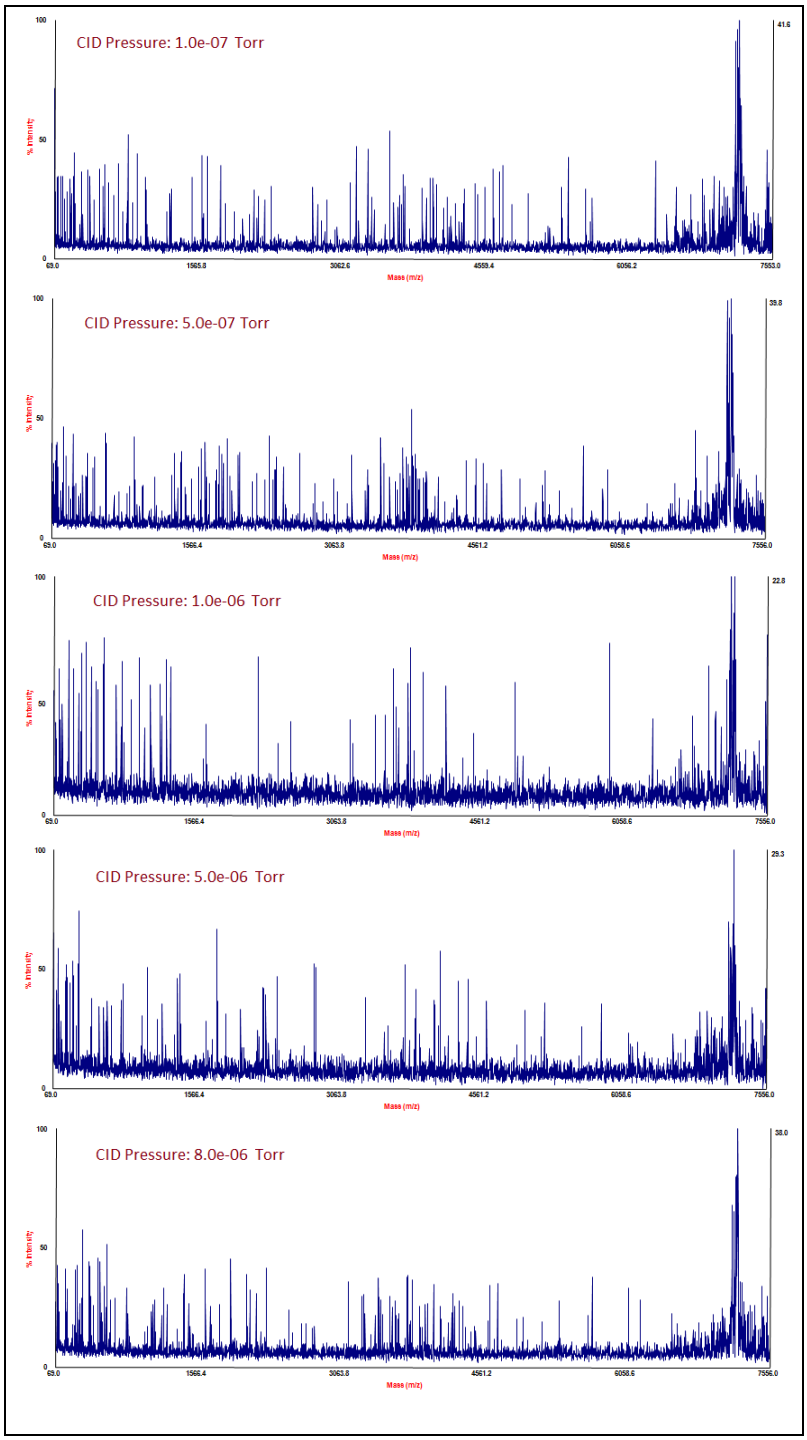

Figure 12. MS/MS spectra of $[miR\text{-}124a + H^+]^+$ ion that were acquired at different CID pressure, $1.0e^{-07}$ – $8.0e^{-06}$ Torr. 20 µM miR-124a was spotted on 3-HPA thin-layer matrix and analyzed using laser intensity = 7500 arb. units.

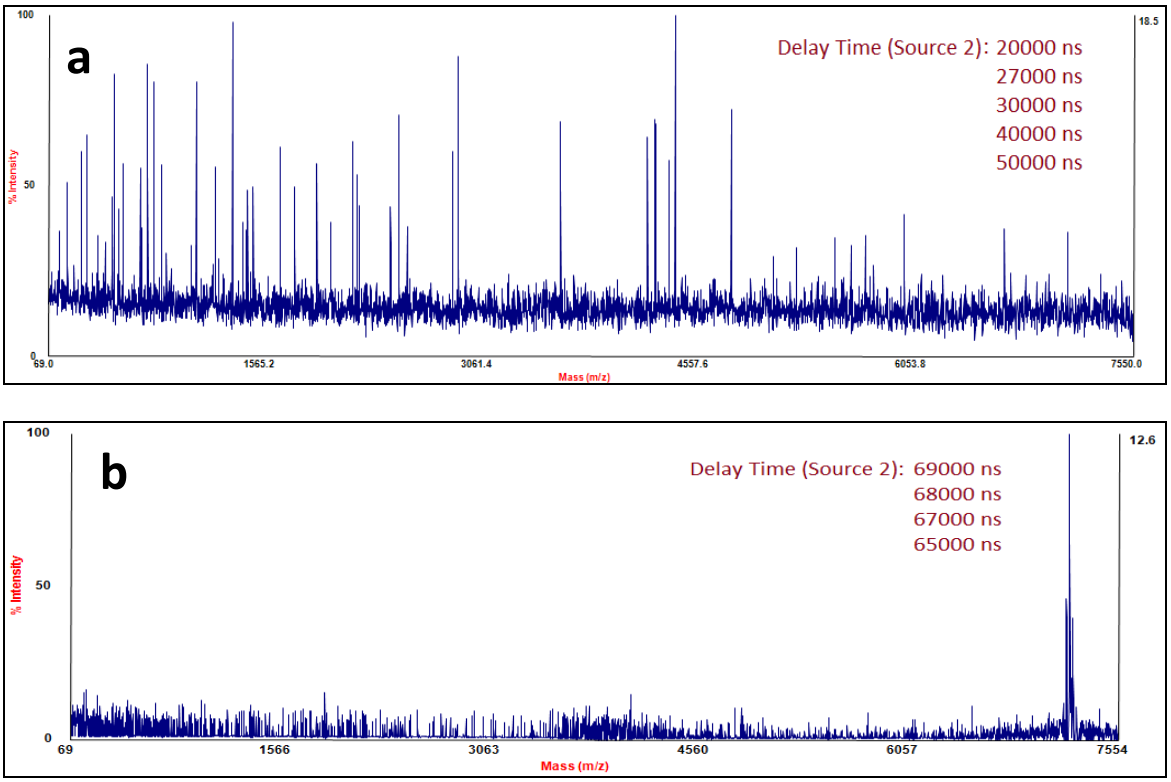

Figure 13. MS/MS spectra of $[miR\text{-}124a + H^+]^+$ that were acquired with low (a) and high (b) duration times for the CID process. 20 µM miR-124a was spotted on 3-HPA thin-layer matrix and analyzed using laser intensity = 7500 arb. units and CID pressure = $1.0e^{-07}$ Torr.

After the extensive optimization of signal intensity of miR-124a precursor ion (laser intensity, concentration of miR-124s, sample preparation method, choice matrix compound and spiking of additional matrix), and the study of various parameters for carrying out MS/MS measurements of miR-124a (positive/negative ion mode, CID pressure and delay time), the production of CID fragments remained insufficient for partial *de novo* sequencing. One of the possible explanations was the singly-charged $[miR\text{-}124a + H^+]^+$ precursor ion and some of its CID fragments (≥4,000 m/z) were too heavy for the current settings in the reflectron, which was an essential component in the instrument for MS/MS measurements. As a result, the efficiency on channeling the ions

to the corresponding reflectron detector was significantly lowered. To overcome this limitation from the reflectron, the doubly charged [miR-124a + $2H^+$]$^{2+}$ ion with a mass-to-charge ratio of 3,581 was used as an alternative precursor ion. An advantage of using the doubly-charged precursor ion is the internal energy would be higher than that of the singly-charged ion. In the MS/MS spectrum of doubly-charged [miR-124a + $2H^+$]$^{2+}$ ion (Figure 14), the ion count of the precursor ion was greatly increased, and peaks that corresponded to some of the CID fragments could be easily detected.

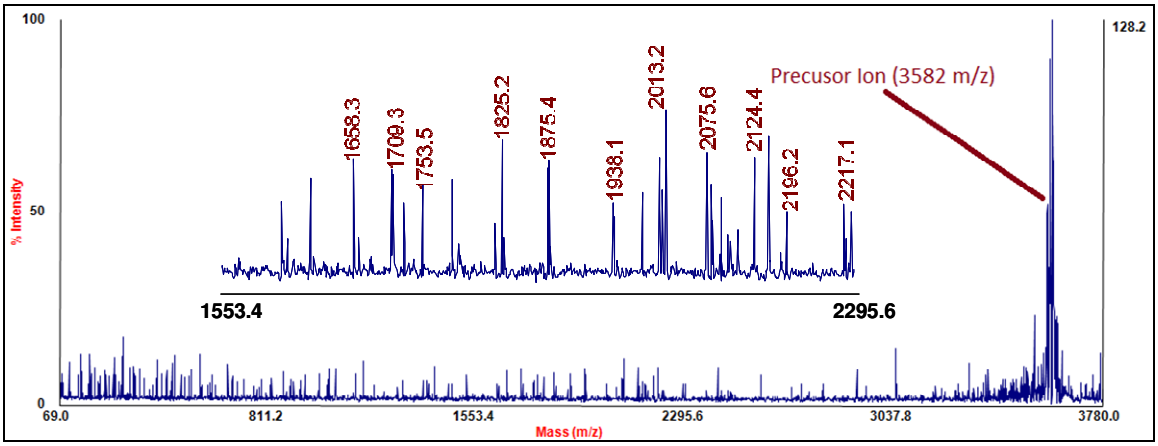

Figure 14. MS/MS spectrum of [miR-124a + $2H^+$]$^{2+}$ precursor ion and its fragment ions.

Post-source decay (PSD) is an alternative approach to induce ion fragmentation. The PSD spectrum of [miR-124a + $2H^+$]$^{2+}$ precursor ion was acquired (Figure 15). The instrumental setup for PSD is exactly the same as MS/MS, except the collision cell is inactivated. Therefore, the CID chamber is maintained at the same high vacuum ($10e^{-8}$ Torr) as in the rest of the MALDI-TOF MS instrument. In the PSD mode, fragmentation of molecular ions occurs while the ions are traveling down the first TOF tube. In

comparison of the PSD spectrum to the MS/MS spectrum (Figure 14), there is increase on signal intensity of most fragment ions, but the numbers of different fragment ions are lowered.

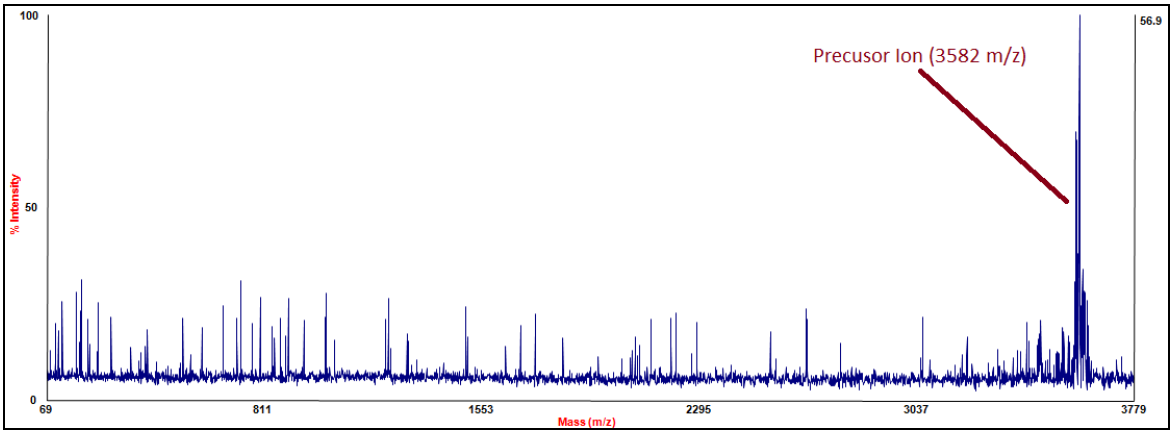

Figure 15. MALDI mass spectrum of [miR-124a + $2H^+$]$^{2+}$ ion that was acquired by using the mode of post-source decay.

Sequence analysis of miR-124a

Microsoft Office Excel was used to perform the calculations of theoretical molecular masses of CID fragments of miR-124a. All expected CID fragments were generated according to the RNA sequence of miR-124a and the fragmentation pattern that has been reported (Figure 3). Manually, the theoretical masses of expected CID fragment ions were compared with the measured masses. Without the proper mass calibration, a mass error of ± 5 Da was acceptable at this early stage. Based on the expected a/w ions, 14% of the measured masses matched with the theorectical masses as shown in Table 8. Whereas, for the expected c/y ions, 31% matching was achieved (Table 9). This complies with the report from Andersen et al., in which they had also observed c/y ions

as the most abundant fragment ions of 4-mer RNA. As far as we are concerned, the above results represented the first attempt to fragment any miRNA that could contain as many as 25 nucleotides by using the high CID energy in MALDI-TOF/TOF MS. Among the a/w and c/y ions, a total of 45% matching of measured masses with the theoretical masses was achieved, thus allowing some of the peaks in Figures 16 and 17 to be identified. The other peaks in Figures 16 and 17 that have not been identified could correspond to other possible fragments, for example a-B ions or internal fragments. However, owing to the double charge on the precursor ion, the data interpretation has become very complex.

Table 8. Identification of (a-w) fragment ions by comparing measured masses to theoretical masses of expected fragment ions

Fragment:	[miR-124a + 2H]$^{2+}$ Raw Spectra:	Theoretical a-Fragment:	5'-Phos to 3'-OH miR-124a Fragment Sequence
a_1	145.8873	154.5961	U
a_2	316.7495	307.6804	UU
a_3	**477.2531**	**472.2850**	**UUA**
a_4	664.2319	636.8895	UUA A
a_5	821.8332	809.4937	UUA AG
a_6	991.3998	982.0979	UUA AGG
a_7	1146.5150	1134.6899	UUA AGG C
a_8	1288.2720	1299.2945	UUA AGG CA
a_9	1463.2783	1451.8865	UUA AGG CAC
a_{10}	1658.3225	1624.4907	UUA AGG CAC G
a_{11}	1767.8491	1777.0827	UUA AGG CAC GC
a_{12}	1938.1310	1949.6869	UUA AGG CAC GCG
a_{13}	**2124.4348**	**2122.2911**	**UUA AGG CAC GCG G**
a_{14}	2293.0203	2275.3754	UUA AGG CAC GCG GU
a_{15}	2408.7510	2447.9796	UUA AGG CAC GCG GUG
a_{16}	2561.4998	2612.5842	UUA AGG CAC GCG GUG A
a_{17}	2707.0781	2777.1887	UUA AGG CAC GCG GUG AA
a_{18}	2903.7593	2930.2731	UUA AGG CAC GCG GUG AAU
a_{19}	3042.3982	3102.8773	UUA AGG CAC GCG GUG AAU G
a_{20}	3303.0486	3255.4693	UUA AGG CAC GCG GUG AAU GC
a_{21}	3422.0947	3408.0613	UUA AGG CAC GCG GUG AAU GCC
	3581.7739	3581.1672	UUA AGG CAC GCG GUG AAU GCC A

Fragment:	[miR-124a + 2H]$^{2+}$ Raw Spectra:	Theoretical w-Fragment:	5'-Phos to 3'-OH miR-124a Fragment Sequence
	3581.7739	3581.1672	UUA AGG CAC GCG GUG AAU GCC A
w_1	3422.0947	3427.5789	UA AGG CAC GCG GUG AAU GCC A
w_2	3303.0486	3274.4946	A AGG CAC GCG GUG AAU GCC A
w_3	3042.3982	3109.8900	AGG CAC GCG GUG AAU GCC A
w_4	2903.7593	2945.2855	GG CAC GCG GUG AAU GCC A
w_5	2707.0781	2772.6813	G CAC GCG GUG AAU GCC A
w_6	2561.4998	2600.0771	CAC GCG GUG AAU GCC A
w_7	2408.7510	2447.4851	AC GCG GUG AAU GCC A
w_8	2293.0203	2282.8805	C GCG GUG AAU GCC A
w_9	2124.4348	2130.2885	GCG GUG AAU GCC A
w_{10}	1938.1310	1957.6843	CG GUG AAU GCC A
w_{11}	1825.2515	1805.0923	G GUG AAU GCC A
w_{12}	1658.3225	1632.4881	GUG AAU GCC A
w_{13}	**1463.2783**	**1459.8839**	**UG AAU GCC A**
w_{14}	1288.2720	1306.7996	G AAU GCC A
w_{15}	1146.5150	1134.1954	AAU GCC A
w_{16}	939.8189	969.5908	AU GCC A
w_{17}	821.8332	804.9863	U GCC A
w_{18}	664.2319	651.9019	GCC A
w_{19}	**477.2531**	**479.2977**	**CC A**
w_{20}	**331.2343**	**326.7057**	**C A**
w_{21}	**175.0853**	**174.1137**	**A**

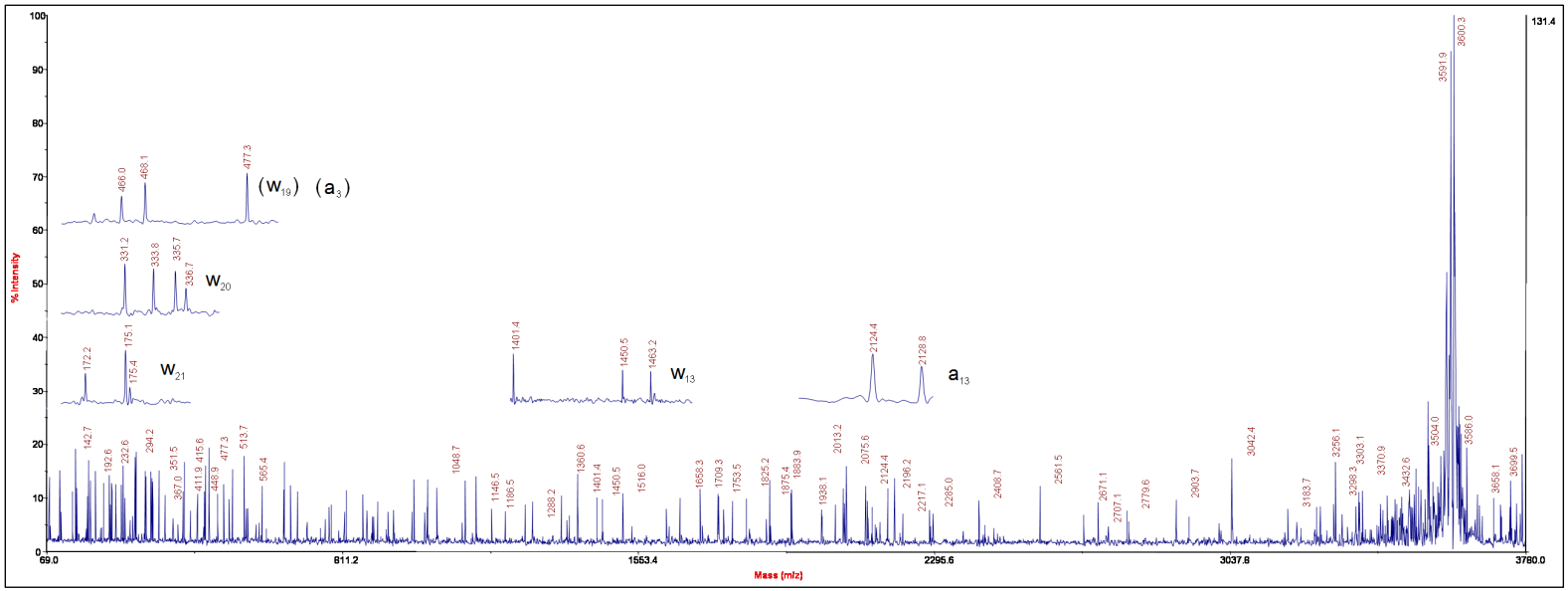

Figure 16. MS/MS spectra of [miR-124a + $2H^+$]$^{2+}$ precursor ion, with selected (a-w) fragment ions being highlighted. Refer to Table 8 to identify fragment sequence and *m/z* ratio for each a- and w- fragment.

Table 9. Identification of (c-y) fragment ions by comparing measured masses to theoretical masses of expected fragment ions

Fragment:	[miR-124a + 2H]$^{2+}$ Raw Spectra:	Theoretical c-Fragment:	5'-Phos to 3'-OH miR-124a Fragment Sequence
c_1	192.6126	194.5793	U
c_2	351.5266	347.6636	UU
c_3	513.7394	512.2682	UUA
c_4	682.0699	676.8727	UUA A
c_5	863.1318	849.4769	UUA AG
c_6	1023.9087	1022.0811	UUA AGG
c_7	1146.5150	1174.6731	UUA AGG C
c_8	1360.6445	1339.2777	UUA AGG CA
c_9	1463.2783	1491.8697	UUA AGG CAC
c_{10}	1658.3225	1664.4739	UUA AGG CAC G
c_{11}	1825.2515	1817.0659	UUA AGG CAC GC
c_{12}	1938.1310	1989.6701	UUA AGG CAC GCG
c_{13}	2179.9497	2162.2743	UUA AGG CAC GCG G
c_{14}	2293.0203	2315.3586	UUA AGG CAC GCG GU
c_{15}	2408.7510	2487.9628	UUA AGG CAC GCG GUG
c_{16}	2707.0781	2652.5674	UUA AGG CAC GCG GUG A
c_{17}	2903.7593	2817.1719	UUA AGG CAC GCG GUG AA
c_{18}	2903.7593	2970.2563	UUA AGG CAC GCG GUG AAU
c_{19}	3042.3982	3142.8605	UUA AGG CAC GCG GUG AAU G
c_{20}	3303.0486	3295.4525	UUA AGG CAC GCG GUG AAU GC
c_{21}	3458.0552	3448.0445	UUA AGG CAC GCG GUG AAU GCC
	3581.7739	3581.1672	UUA AGG CAC GCG GUG AAU GCC A

Fragment:	[miR-124a + 2H]$^{2+}$ Raw Spectra:	Theoretical y-Fragment:	5'-Phos to 3'-OH miR-124a Fragment Sequence
	3581.7739	3581.1672	UUA AGG CAC GCG GUG AAU GCC A
y_1	3370.8938	3387.5958	UA AGG CAC GCG GUG AAU GCC A
y_2	3303.0486	3234.5114	A AGG CAC GCG GUG AAU GCC A
y_3	3042.3982	3069.9069	AGG CAC GCG GUG AAU GCC A
y_4	2903.7593	2905.3023	GG CAC GCG GUG AAU GCC A
y_5	2707.0781	2732.6981	G CAC GCG GUG AAU GCC A
y_6	2561.4998	2560.0939	CAC GCG GUG AAU GCC A
y_7	2408.7510	2407.5019	AC GCG GUG AAU GCC A
y_8	2293.0203	2242.8974	C GCG GUG AAU GCC A
y_9	2075.6077	2090.3054	GCG GUG AAU GCC A
y_{10}	1936.6866	1917.7012	CG GUG AAU GCC A
y_{11}	1767.8491	1765.1092	G GUG AAU GCC A
y_{12}	1658.3225	1592.5050	GUG AAU GCC A
y_{13}	1401.4368	1419.9008	UG AAU GCC A
y_{14}	1288.2720	1266.8164	G AAU GCC A
y_{15}	1048.7485	1094.2122	AAU GCC A
y_{16}	926.0856	929.6077	AU GCC A
y_{17}	784.1602	765.0031	U GCC A
y_{18}	609.7697	611.9188	GCC A
y_{19}	447.6925	439.3146	CC A
y_{20}	291.6314	286.7226	C A
y_{21}	133.8575	134.1306	A

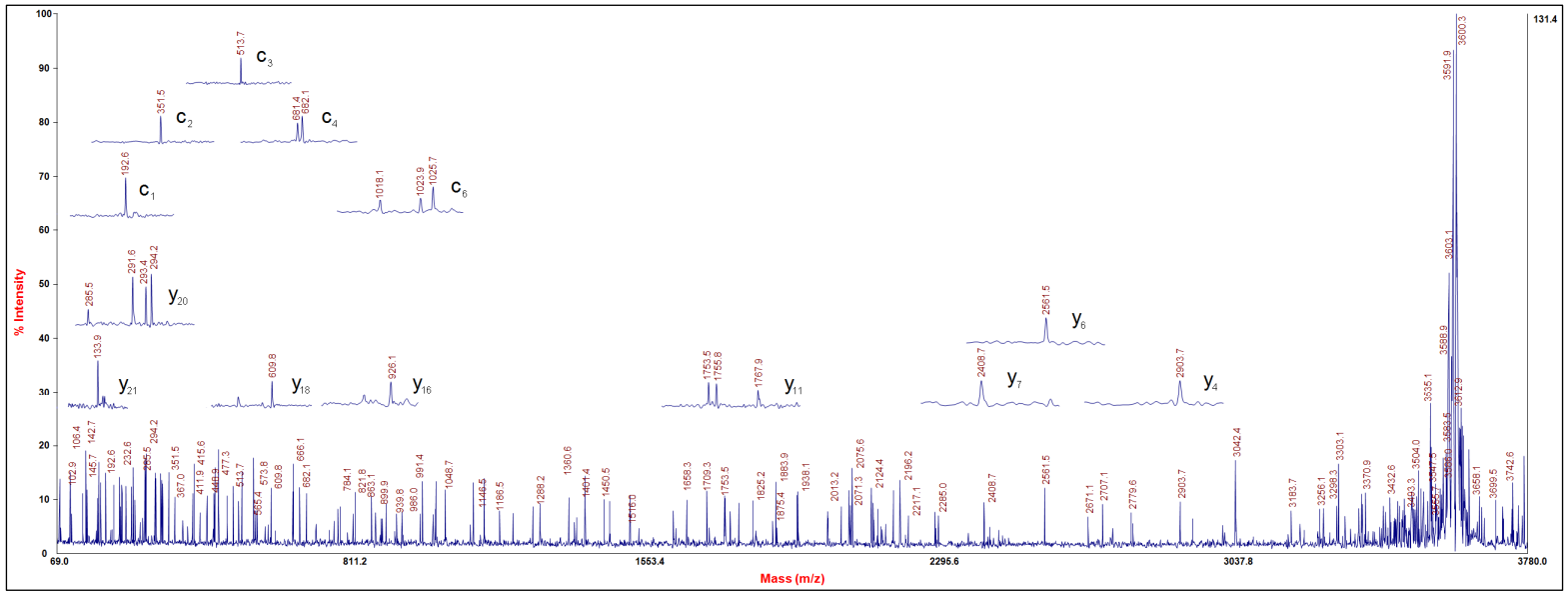

Figure 17. MS/MS spectra of [miR-124a + $2H^+$]$^{2+}$ precursor ion, with selected (c-y) fragment ions being highlighted. Refer to Table 9 to identify fragment sequence and *m/z* ratio for each c- and y- fragment.

CHAPTER IV

CONCLUSIONS

The studies of MALDI-TOF MS in the linear positive ion mode through the investigation of the effects of laser intensity on 3-HPA matrix and miR-124a, concentration of miR-124a, sample preparation methods and using five different MALDI matrix compounds have provided our research group with a great deal of information and understanding on the desorption process of MALDI. These provided our research group and the others within the scientific community a good foundation towards the clinical applications of MALDI-TOF MS in miRNA analysis. In addition, the knowledge generated in this thesis is easily applicable to the analysis of other small non-coding RNA molecules.

Specifically, optimal parameters for linear MALDI-TOF MS and sample preparation method have been determined for miRNA analysis. The comparison study of five different MALDI matrices has demonstrated a correlation between the characteristics of matrix compound and the success of MALDI-TOF MS measurements. The hydrophobicity study showed that as matrix compound increased on its molecular mass which is proportional to the hydrophobicity of the matrix compound. Therefore, small matrix compound would provide less hydrophobic interactions with each other as compared to larger matrix compounds. 50% DMF was confirmed to be the best solvent for for solubilizing the selected matrix compounds and attained sufficiently high molar

concentration to support the MALDI process. 3-HPA matrix allowed for the fastest sample preparation due to having the fastest drying time, compared to the other four matrix compounds. UV absorbance measurements confirmed that DABP has the highest absorptivity at 355 nm. When the results of MALDI-TOF MS measurements were compared, 3-HPA yielded the highest S/N ratio and ion count. The overall comparison study allowed for a better understanding of how the size and structure of a matrix compound could affect the outcome of MALDI-TOF MS analysis.

The $[\text{miR-124a} + 2H^+]^{2+}$ precursor ion provided the best MS/MS spectra for miR-124a sequence analysis. Since the RNA sequence of miR-124a is known and validated, Microsoft Office Excel can therefore be used to calculate the theoretical masses of expected CID fragment ion of miR-124a. The peaks in the MS/MS spectra of either $[\text{miRNA} + H^+]^+$ and $[\text{miRNA} + 2H^+]^{2+}$ precursor ion could be identified by comparing the measured masses with the theoretical masses, thus allowing partial *de novo* sequencing of miR-124a. However, the MS/MS process still needs to be studied further due to the fact that spectral data seems to be irreproducible. The acquisition of two MS/MS spectra might never be the results of exactly the same fragmentation pattern due to the nature of the CID process itself.

REFERENCES

1. Ambros, V.; Lee, R., Identification of microRNAs and other tiny noncoding RNAs by cDNA cloning. *Methods Mol Biol* **2004,** *265*, 131-58.

2. Kadener, S.; Rodriguez, J.; Abruzzi, K.; Khodor, Y.; Sugino, K.; Marr, M. n.; Nelson, S.; Rosbash, M., Genome-wide identification of targets of the drosha-pasha/DGCR8 complex. *RNA* **2009,** *15* (4), 537-45.

3. Piriyapongsa, J.; Mariño-Ramírez, L.; Jordan, I., Origin and evolution of human microRNAs from transposable elements. *Genetics* **2007,** *176* (2), 1323-37.

4. Lee, R.; Feinbaum, R.; Ambros, V., The C. elegans heterochronic gene lin-4 encodes small RNAs with antisense complementarity to lin-14. *Cell* **1993,** *75* (5), 843-54.

5. Gramantieri, L.; Ferracin, M.; Fornari, F.; Veronese, A.; Sabbioni, S.; Liu, C.; Calin, G.; Giovannini, C.; Ferrazzi, E.; Grazi, G.; Croce, C.; Bolondi, L.; Negrini, M., Cyclin G1 is a target of miR-122a, a microRNA frequently down-regulated in human hepatocellular carcinoma. *Cancer Res* **2007,** *67* (13), 6092-9.

6. Zhu, S.; Si, M.; Wu, H.; Mo, Y., MicroRNA-21 targets the tumor suppressor gene tropomyosin 1 (TPM1). *J Biol Chem* **2007,** *282* (19), 14328-36.

7. Griffiths-Jones, S.; Grocock, R.; van Dongen, S.; Bateman, A.; Enright, A., miRBase: microRNA sequences, targets and gene nomenclature. *Nucleic Acids Res* **2006,** *34* (Database issue), D140-4.

8. Mattie, M.; Benz, C.; Bowers, J.; Sensinger, K.; Wong, L.; Scott, G.; Fedele, V.; Ginzinger, D.; Getts, R.; Haqq, C., Optimized high-throughput microRNA expression profiling provides novel biomarker assessment of clinical prostate and breast cancer biopsies. *Mol Cancer* **2006,** *5*, 24.

9. Chen, C.; Ridzon, D.; Broomer, A.; Zhou, Z.; Lee, D.; Nguyen, J.; Barbisin, M.; Xu, N.; Mahuvakar, V.; Andersen, M.; Lao, K.; Livak, K.; Guegler, K., Real-time quantification of microRNAs by stem-loop RT-PCR. *Nucleic Acids Res* **2005,** *33* (20), e179.

10. Liang, R.; Li, W.; Li, Y.; Tan, C.; Li, J.; Jin, Y.; Ruan, K., An oligonucleotide microarray for microRNA expression analysis based on labeling RNA with quantum dot and nanogold probe. *Nucleic Acids Res* **2005,** *33* (2), e17.

11. Barnes, C. A.; Chiu, N. H. L., Accurate characterization of carcinogenic DNA adducts using MALDI tandem time-of-flight mass spectrometry. *International Journal of Mass Spectrometry* **2009,** *279*, 170-175.

12. Andersen, T.; Kirpekar, F.; Haselmann, K., RNA fragmentation in MALDI mass spectrometry studied by H/D-exchange: mechanisms of general applicability to nucleic acids. *J Am Soc Mass Spectrom* **2006,** *17* (10), 1353-68.

13. Zhu, Y.; Chung, C.; Taranenko, N.; Allman, S.; Martin, S.; Haff, L.; Chen, C., The study of 2,3,4-trihydroxyacetophenone and 2,4,6-trihydroxyacetophenone as matrices for DNA detection in matrix-assisted laser desorption/ionization time-of-flight mass spectrometry. *Rapid Commun Mass Spectrom* **1996,** *10* (3), 383-8.

14. Fu, Y.; Xu, S.; Pan, C.; Ye, M.; Zou, H.; Guo, B., A matrix of 3,4-diaminobenzophenone for the analysis of oligonucleotides by matrix-assisted laser desorption/ionization time-of-flight mass spectrometry. *Nucleic Acids Res* **2006,** *34* (13), e94.

15. Xu, S.; Ye, M.; Xu, D.; Li, X.; Pan, C.; Zou, H., Matrix with high salt tolerance for the analysis of peptide and protein samples by desorption/ionization time-of-flight mass spectrometry. *Anal Chem* **2006,** *78* (8), 2593-9.

16. Zhang, Z.; Zhou, L.; Zhao, S.; Deng, H.; Deng, Q., 3-Hydroxycoumarin as a new matrix for matrix-assisted laser desorption/ionization time-of-flight mass spectrometry of DNA. *J Am Soc Mass Spectrom* **2006,** *17* (12), 1665-8.

17. Zagorevskii, D. V.; Aldersley, M. F.; Ferris, J. P., MALDI Analysis of Oligonucleotides Directly from Montmorillonite. *Journal of American Society of Mass Spectrometry* **2006,** *17*, 1265-1270.

18. Song, F., Evidence for involvement of the backbone in the ionization process of nucleic acids by matrix-assisted laser desorption/ionization. *Rapid Commun Mass Spectrom* **2003,** *17* (10), 1095-8.

19. McLuckey, S. A.; Wu, J.; Bundy, J. L.; Stephenson, J. L.; Hurst, G. B., Oligonucleotide mixture analysis via electrospray and ion/ion reactions in a quadrupole ion trap. *Anal Chem* **2002,** *74* (5), 976-84.

20. Taucher, M.; Rieder, U.; Breuker, K., Minimizing base loss and internal fragmentation in collisionally activated dissociation of multiply deprotonated RNA. *J Am Soc Mass Spectrom* **2010,** *21* (2), 278-85.